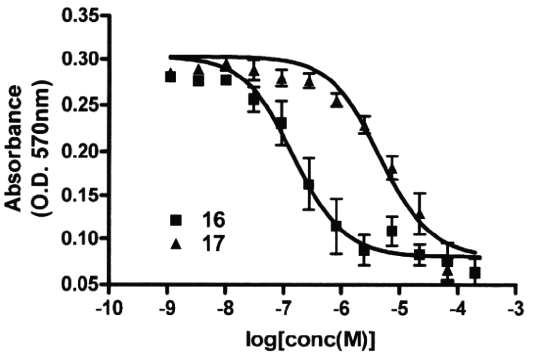

Fig. 2 The inhibitory effect of cyclic RGD peptides on HDF attachment to vitronectin. HDFs were allowed to attach to human vitronectin in the presence of various concentrations of cyclic RGD peptides. Peptides were added to the cell suspension and the cells were plated. After a 30 min incubation period, the attached cells were stained with crystal violet and dissolved in a 1% SDS solution. The absorbance at 570 nm was measured. Triplicate experiments gave similar results.

uncharged amide NH of Gly-Asp is located proximal to the integrin residue Arg216, which is likely to be involved in the interaction.[18] These results suggest that substitution of the Gly-Asp peptide bond with a positively-charged amidine unit partially eliminated the highly potent binding affinity towards the $\alpha_v\beta_3$ integrin.

Conclusion

In conclusion, we have established a novel approach to synthesize acyclic amidine and amide units *via* a key amidoxime (*N*-hydroxyamidine) precursor, which was prepared from a nitrile oxide component as an active ester equivalent. This method was used for the Fmoc-based solid-phase synthesis of peptides and peptidomimetics containing an amidine-type isostere. The peptide aldoxime represented a functional precursor for a protected cyclic peptide and peptidomimetic, suggesting that the nitrile oxide-mediated coupling reaction could serve as an alternative method for peptide macrocyclizations. Further studies on the scope and limitations of this approach, as well as applications for structure–activity relationship studies of bioactive peptides, are currently in progress.

Experimental section

Synthesis

***tert*-Butyl [(*S*)-1-(hydroxyiminomethyl)-2-methylpropyl]carbamate (9).** To a solution of Boc-Val-NMe(OMe) (5.00 g, 19.2 mmol) in Et_2O (60 cm^3) was added dropwise a solution of $LiAlH_4$ (1.02 g, 27.0 mmol) in Et_2O (20 cm^3) at −40 °C and the mixture was stirred for 40 min. The reaction was quenched at −40 °C by the addition of an Na_2SO_4 solution. The reaction mixture was washed with saturated aqueous $NaHCO_3$ and brine, and dried over Na_2SO_4. Concentration under reduced pressure gave the Boc-valinal. To a solution of $NH_2OH{\cdot}HCl$ (1.66 g, 23.9 mmol) and AcONa (1.96 g, 23.9 mmol) in EtOH (50 cm^3) was added the solution of the aldehyde in EtOH (15 cm^3). The reaction mixture was stirred at 80 °C for 15 min. The mixture was concentrated under reduced pressure. The residue was extracted with CH_2Cl_2, and the extract was washed with H_2O and dried over Na_2SO_4. Concentration under reduced pressure followed by flash chromatography over silica gel with n-hexane–EtOAc (3/1) gave the title compounds **9a** and **9b** (3.44 g, 82% yield, **9a**/**9b** = 58/42) both as white solids.

Compound **9a**: mp 35–36 °C; $[\alpha]_D^{26}$ +11.0 (*c* 0.58, $CHCl_3$); δ_H (500 MHz, DMSO, Me_4Si) 0.82 (6H, dd, *J* = 13.7 and 6.9 Hz), 1.37 (9H, s), 1.75 (1H, td, *J* = 13.7 and 6.9 Hz), 3.72–3.78 (1H, m), 6.96 (1H, d, *J* = 8.8 Hz), 7.14 (1H, d, *J* = 7.3 Hz) and 10.63 (1H, s); δ_C (125 MHz, DMSO-d_6, Me_4Si) 18.6, 18.8, 28.2 (3C), 30.9, 55.4, 77.7, 149.0 and 155.1. Anal. calc. for $C_{10}H_{20}N_2O_3$: C, 55.53; H, 9.32; N, 12.95. Found: C, 55.29; H, 9.17; N, 12.81%.

Compound **9b**: mp 114–115 °C; $[\alpha]_D^{26}$ +50.0 (*c* 0.18, $CHCl_3$); δ_H (500 MHz, DMSO-d_6, Me_4Si) 0.81 (6H, t, *J* = 7.2 Hz), 1.37 (9H, s), 1.76–1.85 (1H, m), 4.54 (1H, dd, *J* = 15.7 and 7.1 Hz), 6.51 (1H, d, *J* = 7.1 Hz), 6.95 (1H, d, *J* = 8.9 Hz) and 10.86 (1H, s); δ_C (125 MHz, DMSO, Me_4Si) 18.3, 18.7, 28.2 (3C), 30.7, 50.2, 77.7, 149.9 and 155.2. Anal. calc. for $C_{10}H_{20}N_2O_3$: C, 55.53; H, 9.32; N, 12.95. Found: C, 55.25; H, 9.32; N, 12.71%.

***tert*-Butyl (*S*)-2-{[(*S*)-2-*tert*-butoxycarbonylamino-*N*-hydroxy-3-methylbutanimidoyl]amino}-3-phenylpropionate (13).** To a solution of aldoxime **9b** (30.0 mg, 0.140 mmol) in DMF (0.6 cm^3) was added *N*-chlorosuccinimide (26.2 mg, 0.200 mmol) and the mixture stirred at room temperature for 4 h. The reaction mixture was extracted with EtOAc, the extract washed with a solution of H_2O/brine (1/1) and dried over Na_2SO_4. After concentration under reduced pressure, the residue was dissolved in Et_2O (5 cm^3). To the solution were added Et_3N (77 mm^3, 0.560 mmol) and H-Phe-O^{t}Bu **12** (30.0 mg, 0.140 mmol), and the mixture stirred at room temperature overnight. The reaction mixture was washed with brine and dried over Na_2SO_4. Concentration under reduced pressure followed by flash chromatography over silica gel with n-hexane–EtOAc (3/1) gave title compound **13** (50.0 mg, 81% yield, inseparable mixture of major/minor = 97/3) as a colorless oil: $[\alpha]_D^{26}$ −19.2 (*c* 0.73, $CHCl_3$); δ_H (500 MHz, DMSO-d_6, Me_4Si) 0.63 (3H, d, *J* = 6.6 Hz), 0.73 (3H, d, *J* = 6.6 Hz), 1.32 (9H, s), 1.37 (9H, s), 1.79 (1H, dt, *J* = 21.7 and 6.6 Hz), 2.84–2.94 (2H, m), 3.70 (1H, t, *J* = 9.0 Hz), 4.44–4.52 (1H, m), 5.38 (1H, d, *J* = 10.5 Hz), 6.66 (1H, d, *J* = 9.5 Hz), 7.19–7.29 (5H, m) and 10.86 (1H, s); δ_C (125 MHz, DMSO-d_6, Me_4Si) 18.3, 19.8, 27.5 (3C), 28.2 (3C), 29.8, 55.0, 56.1, 77.8, 80.6, 126.5, 128.0 (3C), 129.5 (2C), 137.0, 150.5, 155.3 and 171.4; HRMS (FAB) *m*/*z* calc. for $C_{23}H_{38}N_3O_5$ ([M + H]$^+$) 436.2811, found 436.2808.

***tert*-Butyl (*S*)-2-{[(*S*)-2-*tert*-butoxycarbonylamino-3-methylbutanimidoyl]amino}-3-phenylpropionate (14).** To a solution of amidoxime **13** (29.1 mg, 0.0670 mmol) in MeOH (1 cm^3) and AcOH (0.011 cm^3) was added RANEY® Ni (0.85 cm^3, slurry in H_2O) and the mixture stirred under an atmosphere of hydrogen at room temperature for 1 h. The mixture was filtered through Celite®. Concentration under reduced pressure followed by flash chromatography over silica gel with n-hexane–EtOAc (3/1) gave title compound **14** (18.9 mg, 67% yield) as a yellow oil: $[\alpha]_D^{26}$ +7.53 (*c* 0.46, $CHCl_3$); δ_H (500 MHz, DMSO-d_6, Me_4Si) 0.76 (6H, dd, *J* = 13.5 and 6.7 Hz), 1.28 (9H, s), 1.38 (9H, s), 1.80–1.88 (1H, m), 2.86 (1H, br s), 2.92 (1H, dd, *J* = 13.5 and 6.9 Hz), 3.77 (1H, br s), 4.26 (1H, br s), 4.99 (1H, d, *J* = 9.5 Hz), 6.16 (1H, br s), 6.96 (1H, d, *J* = 9.5 Hz) and 7.14–7.26 (5H, m); δ_C (125 MHz, DMSO-d_6, Me_4Si) 18.0 (2C), 19.3, 27.5 (3C), 28.2 (3C), 31.0, 37.8, 59.5, 77.8,

78.9, 126.1, 127.9 (2C), 127.9, 129.2 (2C), 138.1, 155.2 and 171.2; HRMS (FAB) *m/z* calc. for $C_{23}H_{38}N_3O_4$ ([M + H]$^+$) 420.2862, found 420.2864.

***tert*-Butyl (*S*)-2-[(*S*)-2-*tert*-butoxycarbonylamino-3-methylbutyrylamino]-3-phenylpropionate (15).** To a solution of amidoxime **13** (35.3 mg, 0.0810 mmol) in MeOH (0.8 cm^3) and H_2O (0.8 cm^3) were added AcOH (0.00800 cm^3, 0.120 mmol) and $NaNO_2$ (8.30 mg, 0.120 mmol). The mixture was stirred at room temperature overnight. The mixture was concentrated under reduced pressure. The residue was extracted with CH_2Cl_2, and the extract was washed with H_2O and dried over Na_2SO_4. Concentration under reduced pressure followed by flash chromatography over silica gel with n-hexane–AcOEt (3/1) gave title compound **15** (21.0 mg, 62% yield) as a white solid: mp 115–116 °C; $[\alpha]_D^{24}$ +60.0 (*c* 0.87, $CHCl_3$); δ_H (500 MHz, DMSO-d_6, Me_4Si) 0.87 (3H, d, *J* = 5.6 Hz), 0.93 (3H, d, *J* = 6.8 Hz), 1.38 (9H, s), 1.45 (9H, s), 2.04–2.14 (1H, m), 3.04–3.11 (2H, m), 3.91 (1H, t, *J* = 6.8 Hz), 4.74 (1H, dd, *J* = 13.8 and 6.2 Hz), 5.16 (1H, d, *J* = 6.6 Hz), 6.30 (1H, d, *J* = 6.2 Hz) and 7.14–7.31 (5H, m); δ_C (125 MHz, DMSO-d_6, Me_4Si) 17.7, 19.2, 27.9 (3C), 28.3 (3C), 38.2, 52.2, 53.6, 55.1, 82.2, 82.3, 126.9, 127.0 (2C), 128.4 (2C), 129.5, 136.0, 170.3 and 171.0; HRMS (FAB) *m/z* calc. for $C_{23}H_{37}N_2O_5$ ([M + H]$^+$) 421.2702, found 421.2702.

H_2N–O-(2-Cl)Trt resin (18). 2-Chlorotrityl resin chloride (loading: 1.31 mmol g^{-1}, 76.3 mg) was reacted with Fmoc–NHOH (128 mg, 0.500 mmol) and pyridine (0.0810 cm^3, 1.00 mmol) in THF (0.8 cm^3) at 60 °C for 6 h. The solution was removed by decantation and the resulting resin washed with a solution of DMF/(^{i}Pr)$_2$NEt/MeOH (17/2/1). The Fmoc protecting group was removed by treating the resin with a DMF/piperidine solution (80/20, v/v). The loading was determined by measuring at 290 nm the UV absorption of the piperidine-treated sample: 0.900 mmol g^{-1}, 89%.

H–Asp(O^{t}Bu)–D-Phe–Val–Arg(Pbf)–Gly–aldoxime-(2-Cl)Trt resin (20). Solid-supported hydroxyamine **18** (loading: 0.900 mmol g^{-1}, 91.6 mg, 0.0820 mmol) was reacted with Fmoc-glycinal (0.500 mmol) in dichloroethane (0.7 cm^3), $HC(OMe)_3$ (0.5 cm^3) and AcOH (0.001 cm^3) at 60 °C for 2 h. The solution was removed by decantation and the resulting resin was washed with DMF to afford resin **19**. Peptide resin **20** was manually constructed using an Fmoc-based solid-phase synthesis on resin **19**. The Fmoc protecting group was removed by treating the resin with a DMF/piperidine solution (80/20, v/v). The Fmoc-protected amino acid (0.500 mmol, 6.1 equiv.) was successively condensed using 1,3-diisopropylcarbodiimide (0.0770 cm^3, 0.500 mmol, 6.1 equiv.) in the presence of *N*-hydroxybenzotriazole (77 mg, 0.500 mmol, 6.1 equiv.) to give resin **20**. The ^{t}Bu ester for Asp and 2,2,4,6,7-pentamethyldihydrobenzofuran-5-sulfonyl (Pbf) for Arg were employed for side-chain protection.

H–Asp(O^{t}Bu)–D-Phe–Val–Arg(Pbf)–Gly–aldoxime (21). Resin **20** was treated with TFA/TIS/CH_2Cl_2 (20 cm^3, 0.5/0.1/99.4) at room temperature for 1.5 h. After removal of the resin by filtration, the filtrate was concentrated under reduced pressure to give crude peptide aldoxime **21** as a yellow oil (74.0 mg, quant. from resin **18**). The crude product was used without further purification.

***Cyclo*[–Arg(Pbf)–Gly–ψ[C(=NOH)NH]–Asp(O^{t}Bu)–D-Phe–Val–] (22).** To a solution of peptide aldoxime **21** (74.0 mg) in DMF (1 cm^3) was added *N*-chlorosuccinimide (14.7 mg, 0.100 mmol). The solution was stirred at room temperature overnight, and then DMF (40 cm^3) and Et_3N (0.4 cm^3) added. The mixture was stirred at room temperature overnight and then concentrated under reduced pressure. The residue was extracted with EtOAc and the extract washed with brine. The organic layer was dried over Na_2SO_4 and concentrated under reduced pressure to give a yellow oil, which was purified by column chromatography over silica gel with CH_2Cl_2–MeOH (95/5) to give **22** (26.9 mg, 36% yield, major/minor = 79/21) as a yellow solid: mp 168–169 °C; $[\alpha]_D^{25}$ –52.7 (*c* 0.28, $CHCl_3$); δ_H (500 MHz, DMSO-d_6, Me_4Si) 0.85 (major, 3H, d, *J* = 6.9 Hz), 0.68 (minor, 3H, t, *J* = 6.4 Hz), 0.73 (major, 3H, d, *J* = 6.7 Hz), 0.72–0.76 (minor, 3H, m), 1.25–1.50 (2H, m), 1.34 (minor, 9H, s), 1.37 (major, 9H, s), 1.36 (minor, 6H, s), 1.41 (major, 6H, s), 1.74–1.76 (2H, m), 2.00 (3H, s), 2.41 (3H, s), 2.47 (3H, s), 2.30–2.50 (2H, m), 2.59 (1H, dd, *J* = 15.9 and 5.9 Hz), 2.82–2.91 (2H, m), 2.96 (2H, s), 3.79 (major, 1H, t, *J* = 7.0 Hz), 3.82–3.88 (minor, 1H, m), 3.98 (major, 1H, dd, *J* = 14.7 and 7.7 Hz), 4.02–4.08 (minor, 1H, m), 4.10–4.14 (minor, 1H, m), 4.16–4.25 (major, 1H, m), 4.50 (major, 1H, dd, *J* = 14.6 and 8.4 Hz), 4.35–4.45 (minor, 1H, m), 4.54–4.65 (major, 1H, m), 4.60–4.75 (minor, 1H, m), 5.17 (minor, 1H, d, *J* = 9.6 Hz), 5.27 (major, 1H, d, *J* = 10.6 Hz), 6.37 (major, 1H, br s), 6.70 (minor, 1H, br s), 7.12–7.33 (5H, m), 7.42–7.53 (1H, m), 8.05–8.14 (2H, m), 8.32 (minor, 1H, d, *J* = 7.3 Hz), 8.45 (major, 1H, d, *J* = 5.9 Hz), 9.17 (minor, 1H, s) and 9.63 (major, 1H, s); δ_C (125 MHz, DMSO-d_6, Me_4Si) 12.1, 12.3, 17.3 (minor), 17.6 (major), 17.8 (major, 2C), 17.9 (minor, 2C), 18.9, 19.0 (major), 19.1 (minor), 21.1, 27.7 (3C), 27.7, 28.3 (major, 2C), 28.8 (minor, 2C), 36.3, 42.5 (2C), 52.0, 52.6, 55.0, 59.8 (minor), 60.3 (major), 62.8, 79.7 (minor), 80.3 (major), 86.3, 116.3, 124.3, 126.5, 128.1 (minor, 2C), 128.2 (major, 2C), 129.1 (major, 2C), 129.3 (minor, 2C), 131.4, 134.2, 137.0, 137.3, 148.9, 156.0, 157.5, 169.3 (major), 169.5 (minor), 170.7, 171.2, 172.2 and 172.4; HRMS (FAB) *m/z* calc. for $C_{43}H_{64}N_9O_{10}S$ ([M + H]$^+$) 898.4497, found 898.4502.

***Cyclo*[–Arg(Pbf)–Gly–Asp(O^{t}Bu)–D-Phe–Val–] (23a).** To a solution of amidoxime **22** (20.0 mg, 0.0220 mmol) in MeOH (0.5 cm^3) and H_2O (0.2 cm^3) were added AcOH (0.00500 cm^3) and $NaNO_2$ (4.60 mg, 0.0660 mmol). The mixture was stirred at room temperature overnight. The mixture was concentrated under reduced pressure. The residue was extracted with EtOAc, and the extract washed with H_2O and dried over $MgSO_4$. Concentration under reduced pressure followed by PTLC purification with CH_2Cl_2–MeOH (95/5) gave title compound **23a** (8.90 mg, 46% yield) as a white solid: mp 247–248 °C; $[\alpha]_D^{25}$ –32.3 (*c* 0.27, MeOH); δ_H (500 MHz, DMSO-d_6, Me_4Si) 0.70 (6H, dd, *J* = 20.7 and 6.7 Hz), 1.18–1.50 (2H, m), 1.34 (9H, s), 1.41 (6H, s), 1.65–1.72 (1H, m), 1.80–1.88 (1H, m), 2.01 (3H, s), 2.36 (1H, dd, *J* = 15.7 and 8.9 Hz), 2.41 (3H, s), 2.46 (3H, s), 2.80 (1H, dd, *J* = 13.7 and 6.6 Hz), 2.91–3.06 (2H, m), 2.96 (2H, s), 3.28 (2H, s), 3.82 (1H, t, *J* = 7.6 Hz), 4.00–4.10 (2H, m), 4.54–4.62 (2H, m), 6.35 (1H, br s), 6.70–6.80 (1H, m), 7.13–7.28 (5H, m), 7.42–7.50 (5H, m), 7.74 (2H, dd, *J* = 11.5 and 8.3 Hz), 7.95 (1H, d, *J* = 8.3 Hz), 8.06 (1H, d, *J* = 7.6 Hz) and 8.36 (1H, dd, *J* = 7.3 and 4.4 Hz); δ_C (125 MHz, DMSO-d_6, Me_4Si) 12.3, 17.6, 18.2, 18.9, 19.2, 25.8, 27.6 (3C), 28.3 (2C), 28.4, 29.7, 36.4, 37.1, 39.8, 42.5, 43.1, 48.9,

52.2, 53.9, 60.1, 80.0, 86.3, 116.3, 119.7, 124.3, 126.2, 128.1 (2C), 129.0 (2C), 130.3, 131.4, 137.3, 156.0, 157.4, 169.1, 169.4, 169.9, 170.8, 171.0 and 171.1; HRMS (FAB) *m/z* calc. for $C_{43}H_{63}N_8O_{10}S$ ([M + H]$^+$) 883.4388, found 883.4397.

***Cyclo*[–Arg(Pbf)–Gly–ψ[C(=NH)NH]-Asp(O^{t}Bu)–D-Phe–Val–] (23b).** To a solution of amidoxime **22** (30.0 mg, 0.0330 mmol) in MeOH (0.6 cm^3) and AcOH (0.006 cm^3) was added RANEY® Ni (0.440 cm^3, slurry in H_2O), and the mixture stirred under a H_2 atmosphere at room temperature for 2 h. The mixture was filtered through Celite®. Concentration under reduced pressure followed by flash chromatography over silica gel with CH_2Cl_2–MeOH (95/5) gave title compound **23b** (27.4 mg, 95% yield) as a colorless oil: $[\alpha]_D^{26}$ –53.3 (*c* 0.14, $CHCl_3$); δ_H (500 MHz, CD_3OD, Me_4Si) 0.74 (6H, dd, *J* = 14.7 and 6.9 Hz), 1.43 (9H, s), 1.45 (6H, s), 1.45–1.52 (1H, m), 1.55–1.60 (1H, m), 1.82–1.89 (1H, m), 1.95–2.00 (1H, m), 2.07 (3H, s), 2.56 (3H, s), 2.59 (1H, d, *J* = 6.6 Hz), 2.77 (1H, dd, *J* = 16.5 and 6.9 Hz), 2.94 (1H, dd, *J* = 13.3 and 6.7 Hz), 2.99 (2H, s), 3.05 (1H, dd, *J* = 13.2 and 9.0 Hz), 3.11–3.18 (1H, m), 3.53 (1H, d, *J* = 15.2 Hz), 3.87 (1H, d, *J* = 6.9 Hz), 4.28 (1H, d, *J* = 15.2 Hz), 4.34–4.37 (1H, m), 4.39–4.45 (1H, m), 4.68 (1H, dd, *J* = 9.0 and 6.9 Hz) and 7.15–7.29 (5H, m); δ_C (125 MHz, CD_3OD, Me_4Si) 12.5, 18.4, 18.7, 19.6, 19.7, 28.4, 28.4, 28.4 (3C), 29.6 (2C), 30.9, 37.9, 38.4, 44.0, 49.5, 49.7, 54.0, 56.4, 62.5, 82.6, 87.7, 118.5, 126.0, 127.9, 129.6 (2C), 130.4 (2C), 132.4, 133.5, 134.4, 138.0, 139.4, 158.1, 160.0, 172.0, 173.3, 173.6, 173.9, 174.2 and 174.3; HRMS (FAB) *m/z* calc. for $C_{43}H_{62}N_9O_9S$ ([M – H]$^-$) 880.4397, found 880.4395.

***Cyclo*[–Arg–Gly–ψ[C(=NH)NH]–Asp–D-Phe–Val–] (17).** Protected amidine **23b** (7.90 mg, 0.00900 mmol) was treated with 1 M TMSBr–thioanisole in TFA (10 cm^3) in the presence of *m*-cresol (0.1 cm^3) and 1,2-ethanedithiol (0.5 cm^3) at 4 °C for 15 min. The mixture was poured into ice-cold dry Et_2O (50 cm^3). The resulting powder was collected by centrifugation and washed three times with ice-cold dry Et_2O. The crude product was purified by preparative HPLC to afford expected peptide **17** as a white powder (5.30 mg, 0.00660 mmol, 73% yield): $[\alpha]_D^{25}$ –129.2 (*c* 0.17, MeOH); δ_H (500 MHz, DMSO-d_6, Me_4Si) 0.70 (3H, d, *J* = 6.6 Hz), 0.74 (3H, d, *J* = 6.6 Hz), 1.32–1.60 (3H, m), 1.73–1.84 (1H, m), 1.88–1.98 (1H, m), 2.59 (1H, dd, *J* = 17.0 and 5.7 Hz), 2.78 (1H, dd, *J* = 13.5 and 6.5 Hz), 2.84 (1H, dd, *J* = 17.2 and 8.2 Hz), 3.00 (1H, dd, *J* = 13.0 and 8.4 Hz), 3.04–3.13 (2H, m), 3.72–3.78 (2H, m), 3.90–3.98 (1H, m), 4.23 (1H, dd, *J* = 13.5 and 8.2 Hz), 4.43 (1H, t, *J* = 16.2 and 7.0 Hz), 4.53–4.60 (1H, m), 4.62–4.68 (1H, m), 6.80–7.40 (2H, br s), 7.16–7.28 (5H, m), 7.72 (1H, t, *J* = 5.7 Hz), 7.93 (1H, dd, *J* = 11.3 and 8.4 Hz), 8.12 (1H, d, *J* = 7.7 Hz), 8.28–8.32 (1H, m), 8.53 (1H, d, *J* = 7.7 Hz), 8.92–8.98 (1H, m), 9.10–9.20 (1H, m) and 9.64 (1H, s); δ_C (125 MHz, DMSO-d_6, Me_4Si) 17.9, 25.3, 28.2, 29.6, 34.2, 37.0, 37.1, 40.2, 51.7, 51.9, 54.2, 59.9, 126.4, 128.2 (2C), 129.1 (2C), 137.2, 156.8, 158.4, 164.8, 166.8, 170.7, 171.2, 171.3 and 171.7; HRMS (FAB) *m/z* calc. for $C_{26}H_{40}N_9O_6$ ([M + H]$^+$) 574.3102, found 574.3101.

***Cyclo*(–Arg–Gly–Asp–D-Phe–Val–) (16).** By an identical procedure to that described for the preparation of **17**, **23a** (8.00 mg, 0.00900 mmol) was converted into cyclic RGD peptide **16** (0.00790 mmol, 87% yield). All characterization data were in agreement with the data for the control peptide, which was synthesized using Fmoc-based solid-phase synthesis. $[\alpha]_D^{25}$ –21.6 (*c* 0.27, MeOH); δ_H (500 MHz, DMSO-d_6, Me_4Si) 0.68 (3H, d, *J* = 6.7 Hz), 0.75 (3H, d, *J* = 6.7 Hz), 1.32–1.45 (2H, m), 1.45–1.55 (1H, m), 1.69–1.80 (1H, m), 1.80–1.90 (1H, m), 2.38 (1H, dd, *J* = 16.4 and 5.5 Hz), 2.72 (1H, dd, *J* = 16.4 and 8.9 Hz), 2.81 (1H, dd, *J* = 13.5 and 6.1 Hz), 2.94 (1H, dd, *J* = 13.5 and 8.0 Hz), 3.05–3.14 (2H, m), 3.26 (1H, dd, *J* = 15.2 and 4.2 Hz), 3.82 (1H, t, *J* = 7.4 Hz), 4.04 (1H, dd, *J* = 15.2 and 7.7 Hz), 4.08–4.16 (1H, m), 4.55 (1H, dd, *J* = 14.2 and 7.2 Hz), 4.60–4.68 (1H, m), 6.58–7.11 (1H, br s), 7.15–7.25 (5H, m), 7.58 (1H, t, *J* = 5.7 Hz), 7.78 (1H, d, *J* = 7.4 Hz), 7.87 (1H, d, *J* = 8.0 Hz), 8.00 (1H, d, *J* = 7.4 Hz), 8.08 (1H, d, *J* = 8.6 Hz), 8.36 (1H, dd, *J* = 7.4 and 4.2 Hz) and 12.3 (1H, s); δ_C (125 MHz, DMSO-d_6, Me_4Si) 18.1, 19.1, 25.3, 28.2, 29.5, 34.8, 37.1, 40.2, 43.0, 48.8, 52.0, 53.9, 60.1, 126.1, 128.0 (2C), 129.0 (2C), 137.3, 156.6, 158.3, 169.4, 169.8, 170.6, 171.1 and 171.6; HRMS (FAB) *m/z* calc. for $C_{26}H_{39}N_8O_7$ ([M + H]$^+$) 575.2942, found 575.2952.

Evaluation of inhibitory activity against integrin-mediated cell attachment. Human dermal fibroblasts (HDFs; AGC Techno Glass, Chiba, Japan) were maintained in DMEM containing 10% FBS, 100 U cm^{-3} penicillin and 100 μg cm^{-3} streptomycin (Invitrogen, Carlsbad, CA, USA). Human plasma vitronectin (0.1 μg in 0.050 cm^3 well^{-1}; EMD Chemicals Inc., Gibbstown, NJ, USA) were added to 96-well plates (Nalge Nunc, Rochester, NY, USA) and incubated for 1 h at 37 °C. The plates were washed and blocked with 1% bovine serum albumin (BSA; Sigma-Aldrich, St. Louis, MO, USA) in DMEM. HDFs were incubated at room temperature for 15 min in various concentrations of peptides (0.001–200 μM in 1% DMSO). Then, 0.100 cm^3 HDFs (2×10^4 cells) in DMEM containing 0.1% BSA were added to each well and incubated at 37 °C for 30 min in 5% CO_2. The attached cells were stained with a 0.2% crystal violet aqueous solution in 20% MeOH (0.150 cm^3) for 15 min. After washing with Milli-Q water, the plates were dried overnight at room temperature and dissolved in 0.150 cm^3 of a 1% SDS solution. The absorbance at 570 nm was measured. Each sample was assayed in triplicate, and cells attached to the BSA were subtracted from all measurements. 1% DMSO did not have any effect on HDF attachment to vitronectin.

Acknowledgements

This work was supported by Grants-in-Aid for Scientific Research and the Targeted Protein Research Program from the Ministry of Education, Culture, Sports, Science, and Technology of Japan. E. I. and K. T. are grateful for Research Fellowships from the JSPS for Young Scientists.

Notes and references

1 For reviews, see: (*a*) K. Burgess, *Acc. Chem. Res.*, 2001, **34**, 826; (*b*) M. G. Bursavich and D. H. Rich, *J. Med. Chem.*, 2002, **45**, 541; (*c*) V. J. Hruby, *J. Med. Chem.*, 2003, **46**, 4215.

2 (*a*) R. J. Abraham, S. L. R. Ellison, P. Schonholzer and W. A. Thomas, *Tetrahedron*, 1986, **42**, 2101; (*b*) T. E. Christos, A. Arvanitis, G. A. Cain, A. L. Johnson, R. S. Pottorf, S. W. Tam and W. K. Schmidt, *Bioorg. Med. Chem. Lett.*, 1993, **3**, 1035; (*c*) J. A. K. Howard, V. J. Hoy, D. O'Hagan and G. T. Smith, *Tetrahedron*, 1996, **52**, 12613; (*d*) J. Lin, P. J. Toscano and J. T. Welch, *Proc. Natl. Acad. Sci. U. S. A.*, 1998, **95**, 14020; (*e*) P. Wipf, T. C. Henninger and S. J. Geib, *J. Org. Chem.*, 1998, **63**, 6088.

3 K. A. Newlander, J. F. Callahan, M. L. Moore, T. A. Tomaszek, Jr. and W. F. Huffman, *J. Med. Chem.*, 1993, **36**, 2321.
4 J.-M. Hah, P. Martásek, L. J. Roman and R. B. Silverman, *J. Med. Chem.*, 2003, **46**, 1661.
5 (*a*) M. M. Vasbinder, E. R. Jarvo and S. J. Miller, *Angew. Chem., Int. Ed.*, 2001, **40**, 2824; (*b*) C. L. Jenkins, M. M. Vasbinder, S. J. Miller and R. T. Raines, *Org. Lett.*, 2005, **7**, 2619; (*c*) H. Tamamura, K. Hiramatsu, S. Ueda, Z. Wang, S. Kusano, S. Terakubo, J. O. Trent, S. C. Peiper, N. Yamamoto, H. Nakashima, A. Otaka and N. Fujii, *J. Med. Chem.*, 2005, **48**, 380; (*d*) A. Niida, K. Tomita, M. Mizumoto, H. Tanigaki, T. Terada, S. Oishi, A. Otaka, K. Inui and N. Fujii, *Org. Lett.*, 2006, **8**, 613; (*e*) J. Xiao, B. Weisblum and P. Wipf, *J. Am. Chem. Soc.*, 2005, **127**, 5742.
6 (*a*) S. Oishi, K. Miyamoto, A. Niida, M. Yamamoto, K. Ajito, H. Tamamura, A. Otaka, Y. Kuroda, A. Asai and N. Fujii, *Tetrahedron*, 2006, **62**, 1416; (*b*) S. Oishi, H. Kamitani, Y. Kodera, K. Watanabe, K. Kobayashi, T. Narumi, K. Tomita, H. Ohno, T. Naito, E. Kodama, M. Matsuoka and N. Fujii, *Org. Biomol. Chem.*, 2009, **7**, 2872; (*c*) T. Narumi, R. Hayashi, K. Tomita, K. Kobayashi, N. Tanahara, H. Ohno, T. Naito, E. Kodama, M. Matsuoka, S. Oishi and N. Fujii, *Org. Biomol. Chem.*, 2010, **8**, 616.
7 For acyclic amidine-type peptide isostere, see: H. Moser, A. Fliri, A. Steiger, G. Costello, J. Schreiber and A. Eschenmoser, *Helv. Chim. Acta*, 1986, **69**, 1224.
8 For cyclic amidine-type peptide isosteres, see: (*a*) R. C. F. Jones and G. J. Ward, *Tetrahedron Lett.*, 1988, **29**, 3853; (*b*) P. D. Edwards, J. S. Albert, M. Sylvester, D. Aharony, D. Andisik, O. Callaghan, J. B. Campbell, R. A. Carr, G. Chessari, M. Congreve, M. Frederickson, R. H. A. Folmer, S. Geschwindner, G. Koether, K. Kolmodin, J. Krumrine, R. C. Mauger, C. W. Murray, L.-L. Olsson, S. Patel, N. Spear and G. Tian, *J. Med. Chem.*, 2007, **50**, 5912.
9 M. J. Fisher, U. Giese, C. S. Harms, M. D. Kinnick, T. D. Lingstrom, J. R. McCowan, H.-J. Mest, J. M. Morin, Jr., J. T. Mullaney, M. Paal, A. Rapp, G. Rühter, K. J. Ruterbories, D. J. Sall, R. M. Scarborough, T. Schotten, W. Stenzel, R. D. Towner, S. L. Um, B. G. Utterback, V. L. Wyss and J. A. Jakubowski, *Bioorg. Med. Chem. Lett.*, 2000, **10**, 385.
10 V. A. Vaillancount, S. D. Larsen, S. P. Tanis, J. E. Burr, M. A. Connell, M. M. Cudahy, B. R. Evans, P. V. Fisher, P. D. May, M. D. Meglasson, D. D. Robinson, F. C. Stevens, J. A. Tucker, T. J. Vidmar and J. H. Yu, *J. Med. Chem.*, 2001, **44**, 1231.
11 (*a*) K. W. J. Baker, K. S. Horner, S. A. Moggach, M. Paton and I. A. S. Smellie, *Tetrahedron Lett.*, 2004, **45**, 8913; (*b*) K. C. Fylaktakidou, D. J. Hadjipavlou-Litina, K. E. Litinas, E. A. Varella and D. N. Nicolaides, *Curr. Pharm. Des.*, 2008, **14**, 1001.
12 G. Sauvé, V. S. Rao, G. Lajoie and B. Belleau, *Can. J. Chem.*, 1985, **63**, 3089.
13 Y. J. Chung, E. J. Ryu, G. Keum and B. H. Kim, *Bioorg. Med. Chem.*, 1996, **4**, 209.
14 Compounds **9** were prepared from Boc-valinal according to literature procedures. See: (*a*) A. P. Kozikowski, *Acc. Chem. Res.*, 1984, **17**, 410; (*b*) C. Pichon, K. R. Clemens, A. R. Jacobson and A. I. Scott, *Tetrahedron*, 1992, **48**, 4687.
15 (*a*) R. Haubner, W. Schmitt, G. Hölzemann, S. L. Goodman, A. Jonczyk and H. Kessler, *J. Am. Chem. Soc.*, 1996, **118**, 7881; (*b*) P. Shaffner and M. M. Dard, *Cell. Mol. Life Sci.*, 2003, **60**, 119.
16 Racemization (20%) was observed when Fmoc–D-Phe–H was utilized for on-resin aldoxime formation under the conditions of Table 2, entry 5.
17 R. Bollhagen, M. Schmiedberger, K. Barlos and E. Grell, *J. Chem. Soc., Chem. Commun.*, 1994, 2559.
18 J.-P. Xiong, T. Stehle, R. Zhang, A. Joachimiak, M. Frech, S. L. Goodman and M. A. Arnaout, *Science*, 2002, **296**, 151.

GLIA

GLIA 59:997–1007 (2011)

HIV-1 gp120 Enhances Outward Potassium Current via CXCR4 and cAMP-Dependent Protein Kinase A Signaling in Cultured Rat Microglia

CHANGSHUI XU,[1,2] JIANUO LIU,[1] LINA CHEN,[1] SHANGDONG LIANG,[2] NOBUTAKA FUJII,[3] HIROKAZU TAMAMURA,[4] AND HUANGUI XIONG[1]*

[1]*Neurophysiology Laboratory, Department of Pharmacology and Experimental Neuroscience, University of Nebraska Medical Center, Omaha, Nebraska*

[2]*Department of Physiology, Basic Medical Institute of Nanchang University, Nanchang 330006, People's Republic of China*

[3]*Graduate School of Pharmaceutical Sciences, Kyoto University, Kyoto 606-8501, Japan*

[4]*Department of Molecular Recognition, Institute of Biomaterials and Bioengineering, Tokyo Medical and Dental University, Tokyo 101-0062, Japan*

KEY WORDS

chemokine receptors; voltage-gated K^+ channels; neuronal apoptosis; neurodegeneration

ABSTRACT

Microglia are critical cells in mediating the pathophysiology of neurodegenerative disorders such as HIV-associated neurocognitive disorders. We hypothesize that HIV-1 glycoprotein 120 (gp120) activates microglia by enhancing outward K^+ currents, resulting in microglia secretion of neurotoxins, consequent neuronal dysfunction, and death. To test this hypothesis, we studied the effects of gp120 on outward K^+ current in cultured rat microglia. Application of gp120 enhanced outward K^+ current in a dose-dependent manner, which was blocked by voltage-gated K^+ (K_v) channel blockers. Western blot analysis revealed that gp120 produced an elevated expression of K_v channel proteins. Examination of activation and inactivation of outward K^+ currents showed that gp120 shifted membrane potentials for activation and steady-state inactivation. The gp120-associated enhancement of outward K^+ current was blocked by either a CXCR4 receptor antagonist T140 or a specific protein kinase A (PKA) inhibitor H89, suggesting the involvement of chemokine receptor CXCR4 and PKA in gp120-mediated enhancement of outward K^+ current. Biological significance of gp120-induced enhancement of microglia outward K^+ current was demonstrated by experimental results showing the neurotoxic activity of gp120-stimulated microglia, evaluated by TUNEL staining and MTT assay, significantly attenuated by K_v channel blockers. Taken together, these results suggest that gp120 induces microglia neurotoxic activity by enhancing microglia outward K^+ current and that microglia K_v channels may function as a potential target for the development of therapeutic strategies.

INTRODUCTION

Microglia represent a population of resident immune cells in the brain. They are morphologically, immunophenotypically, and functionally related to cells of the monocyte/macrophage lineage and play an important role as resident immunocompetent phagocytic cells in the pathogenesis of infectious, inflammatory, and degenerative brain diseases. Upon challenging, microglia react by withdrawing their processes, becoming amoeboid and macrophage-like and undergo dramatic phenotypic, immunochemical, and functional changes, collectively referred to as "activation." The switch from resting to activation is characterized by an alteration of functional state. Resting microglia secrete neurotrophic factors, such as NGF, to support neuronal function and survival (Elkabes et al., 1998; Miwa et al., 1997). In contrast, the activated microglia produce reactive oxygen and nitrogen species and pro-inflammatory cytokines and chemokines with potential toxicity to neurons. Moreover, microglia express numerous chemokine receptors which are involved in cell migration and serve as co-receptors for HIV-1 infection. Indeed, microglia are the predominant resident CNS cell type productively infected by HIV-1 (Lipton and Gendelman, 1995). Due to poor penetration of antiviral drugs through blood-brain barrier, resident microglia (and brain macrophages) constitute a cellular reservoir of HIV-1 in the brain and a source of potential neurotoxic products (Gendelman et al., 1997; Genis et al., 1992; Koenig et al., 1986). Studies have shown that HIV-1-infected and immune-activated microglia (and brain macrophages) release a number of soluble substances including, but not limited to, pro-inflammatory cytokines, chemokines, excitatory amino acids, nitric oxide, and reactive oxygen species, as well as viral proteins, which can injure or kill neurons, contributing to the pathogenesis of HIV-1-associated neurocognitive disorders (HAND)(Garden, 2002; Kaul et al., 2001; Kielian, 2004). As such, it is imperative to identify potential target(s) for the development of therapeutic strategies to control microglia activation and/or suppress their subsequent neurotoxin production.

Increasing evidence indicates that voltage-gated K^+ (K_v) channels play a pivotal role in the process of micro-

Grant sponsor: NIH; Grant numbers: R01 NS041862-9 and 5 R01 NS063878.

*Correspondence to: Huangui Xiong, M.D., Ph.D., Department of Pharmacology and Experimental Neuroscience, University of Nebraska Medical Center, Omaha, NE 68198-5880, USA. E-mail: hxiong@unmc.edu

Received 26 May 2010; Accepted 23 February 2011

DOI 10.1002/glia.21171

Published online 24 March 2011 in Wiley Online Library (wileyonlinelibrary.com).

glia activation (Farber and Kettenmann, 2005; Walz and Bekar, 2001). Non-activated microglia express little, if any, K_v channels whereas large outward K^+ current has been observed in activated microglia (Farber and Kettenmann, 2005). Exposure to a variety of activating stimuli produces a similar pattern of electrophysiological changes in microglia. For example, lipopolysaccharide (LPS), macrophage colony-stimulating factor or interferon-γ enhances outward K^+ current in microglia (Eder et al., 1995; Fischer et al., 1995; Norenberg et al., 1994). These outward K^+ currents, which share many properties with cloned $K_v1.3$ channels, including an activation threshold at about −40 mV, strongly use-dependent inactivation, and high sensitivity to 4-aminopyridine (4-AP), agitoxin, margatoxin, and charybdotoxin (Eder et al., 1995; Fordyce et al., 2005; Norenberg et al., 1994), are predominantly recorded in activated microglia (Kotecha and Schlichter, 1999; Menteyne et al., 2009), suggesting a role for K_v channels in regulating microglia activation and cytotoxin production. It has also been shown that K_v channels expressed by activated microglia regulate their proliferation and migration (Kotecha and Schlichter, 1999; Pannasch et al., 2006). Indeed, activated microglia injure neurons, and a blockade of microglia K_v channels inhibits microglia-induced neurotoxicity (Fordyce et al., 2005). These findings stimulate our hypothesis that HIV-1 infection activates microglia by enhancing outward K^+ currents, resulting in microglia production of neurotoxins and consequent neuronal dysfunction and injury. In this study, we tested our hypothesis by exploring the effects of HIV-1 glycoprotein 120 (gp120) on outward K^+ current recorded in cultured rat microglia. Our results showed that gp120 enhanced microglia outward K^+ current via CXCR4 and cAMP-dependent protein kinase A (PKA) signaling pathway, leading to microglia production of neurotoxins and resultant neuronal apoptosis.

MATERIALS AND METHODS

Materials

HIV-1gp120 IIIB was purchased from Immunodiagnostics (Woburn, MA). Aliquots of gp120 were kept as 100 nM stock solution at −80°C. The stock solution was diluted to desired concentrations with artificial cerebrospinal fluid (ACSF) 2–5 min before tests. T140 was kindly provided by Professor Nobutaka Fujii (Kyoto, Japan). All chemicals, unless otherwise specified, were from Sigma (St. Louis, MO).

Isolation and Culture of Microglia and Cortical Neurons

Microglia and cortical neuronal cultures were obtained from the cerebral cortices of 1–2 days old or embryonic (E18) Sprague-Dawley rats (Charles River Laboratories, Wilmington, MA). Briefly, the pups were anesthetized hypothermically and decapitated, and cerebral cortices were dissected out. The cortical tissues were enzymatically digested followed by mechanical dissociation. The mixed primary cultures were grown on 75 cm^2 flasks in 30 mL (10^6 cells/mL) DMEM supplemented with 10% FBS, 2 mM glutamine, and 1% PEN/Strep (37°C, 5%CO_2). After 7–10 days in culture, microglial cells were harvested by gentle shaking, and then plated on uncoated 35 mm plastic Petri dishes at a density of 0.5 × 10^6 cells per dish. Non-adhering cells were removed 30 min after plating by changing the medium. The purity of resulting culture was judged by staining with OX-42 antibody (a marker for the microglia CR3/CD11b receptor). Cells were utilized for whole-cell recording 2 days after plating. In all cases, the culture medium was replaced with fresh ACSF on experimental day. Experiments were conducted 1–2 h after treatment with the reagents. Controls were performed in untreated and age-matched microglial cultures. For cortical neuronal cultures, the cells were plated in poly-D-lysine coated 24 well plates containing 1 mL of medium, with a cell density of 1.0 × 10^5/mL. The cultures were maintained in neurobasal medium supplemented with 1% penicillin/streptomycin, B27(2%, v/v, Invitrogen, San Diego, CA), and L-glutamine (0.5 mM) for at least 7–10 days before being used for experiments. All animal use procedures were strictly reviewed by the Institutional Animal Care and Use Committee (IACUC) of the University of Nebraska Medical Center (IACUC No. 00-062-07).

Electrophysiology

Whole-cell outward K^+ currents were recorded from cultured microglia using an Axopatch 200B amplifier. After establishment of the whole-cell configuration, the cells were allowed to stabilize for 3–5 min before recording. The recorded cells were voltage-clamped at −60 mV and whole-cell outward K^+ current was induced by voltage steps from the holding potential of −60 to −40 mV in the first step, then stepped to +60 mV in increments of 10 mV. The ACSF contained (in mM): 140 NaCl, 5 KCl, 2.0 $CoCl_2$, 1 $MgCl_2$, 10 D-glucose, 10 HEPES (pH 7.4 adjusted with NaOH, osmolarity: 310 mOsm). The recording electrodes were made from borosilcate glass capillaries and had resistance of 5–7.5 MΩ when filled with an intracellular solution contained (in mM): 135 K-gluconate, 10 KCl, 1 $CaCl_2$, 1 $MgCl_2$, 10 EGTA, 0.5 Tris-GTP, 2 Mg-ATP,10 HEPES (Adjusted pH to 7.3 with KOH, osmolarity: 300 mOsm). The seal resistance was 1–10 GΩ. Junction potentials were corrected and the cell capacitance was compensated (~ 70%) in most cells. Current signals were filtered at 1 kHz and digitized at 5 kHz using a Digidata 1440A digitizer. The current and voltage traces were displayed and recorded in a Dell computer using pCLAMP 10 data acquisition/analysis system.

The activation was studied by measuring the peak K^+ conductance (G) during a 700 ms test pulse by varying test potentials from a holding potential of −60 mV. G was calculated starting from $G = I_{peak}/V$, where I_{peak} is the peak outward K^+ current during the test potential (V). Data were normalized to maximum peak conductance (G_{max}) and fitted to Boltzmann equation: G/G_{max} =

$1/[1 + \exp(V - V_{1/2})/k]$, where $V_{1/2}$ is the voltage for half maximal activation, and k is the slope constant (mV). To study steady-state inactivation, cells were held at prepulse potentials ranging from −80 to +10 mV for 60 s and then subject to a +20 mV test pulse for 200 ms. Normalized steady-state currents were plotted versus prepulse potentials, and the curves were fitted by the Boltzmann function: $I/I_{max} = 1/[1 + \exp(V_{pp} - V_{1/2})/k]$, where I_{max} is the maximum current, $V_{1/2}$ is the voltage for half maximal activation, and V_{pp} is the voltage of the prepulse potential.

Immunocytochemistry

Immunocytochemistry was performed to substantiate the capacity of gp120 enhancing expression of microglia K_v channel, particularly $K_v1.3$. Microglia were platted on poly-D-lysine coated coverslips at a density of 0.5×10^6 cells per well in 24 well plates. Twenty-four hour later, microglia were activated by gp120 with or without tetraethylammonium (TEA, 5 mM) or 4-AP (1 mM). After another 24 h, the microglia were washed in PBS three times, fixed with 4% paraformaldehyde (PFA) for 30 min at room temperature. After washing, the microglia were blocked and permeabilized in PBS containing 10% normal goat serum, 0.2% Triton X-100, and 0.1M glycine for 30 min. Primary antibodies, including rat polyclonal antibody Mac-1 (CD11b; 1/500; Serotec) and rabbit polyclonal antibody to $K_v1.3$ (Almonade Lab, Israel), were diluted in PBS with 10% goat serum and applied to coverslips for 1 h. After washing in PBS (5 min, 3 times) Alexa Fluor 488 and Alexa Fluor 594-conjugated secondary antibodies were added for 1 h. Coverslips were mounted on slides with ProLong Gold antifade reagent +DAPI (Molecular Probes), and images were taken with a 40× oil-immersion objective.

Microglia and Neuronal Co-Culture and TUNEL Assay

TUNEL assay was performed using the *in situ* cell death detection kit, AP (Roche Applied Science, Indianapolis, IN). Rat microglia were seeded on transwell inserts (0.5×10^6 cells per well) in 24 well plates and left untreated or exposed to LPS (0.5 μg/mL, as a positive control), gp120 or gp120 plus 4-AP/TEA/H89/T140. Twenty-four hour later, microglia were washed and co-cultured with cortical neurons growing on poly-D-lysine coated coverslips at a density of 1.0×10^5 cells/well in 24-well plates for 24 h. The cortical neurons were then washed in PBS (5 min, 3 times) and fixed with 4% PFA in PBS (pH 7.4) for 1 h at room temperature. After washing three times with PBS, neurons were permeabilized with 0.1% Triton X-100 in 0.1% sodium citrate for 2 min on ice and then washed in PBS (5 min, 3 times). The neurons were then incubated with TUNEL reaction mixture that consisting of terminal deoxynucleotide transferase and fluorescein-labeled nucleotides for incorporation into DNA strand breaks at 37°C. After a final wash in PBS (5 min, 3 times), coverslips were mounted in ProLong Gold antifade reagent with DAPI (Molecular Probes, Eugene, OR). Cells were visualized by Zeiss LSM 510 META NLO microscope an a 40× oil-immersion objective. TUNEL positive cells were counted and expressed as a percentage of total number of cells counted.

MTT Assay

The assay is based on the ability of active mitochondrial dehydrogenase to convert dissolved MTT to water-insoluble purple formazan crystals. Neurons washed in PBS (5 min, 3 times) were incubated with fresh neuronal culture media containing MTT (500 μg/mL) for 3 h. At the end of incubation, the MTT solution was replaced with 500 μL of dimethyl sulfoxide (DMSO) for cell lysis. The plate was shaken for 10 min to solubilize the formazan crystals, and the optical density (OD) at 570 nm was measured.

Statistical Analysis

Experimental data were expressed as mean ± SEM. Statistical analyses were performed by ANOVA or Student t tests. A minimum P value of 0.05 was estimated as the significance level for all tests.

RESULTS

Expression of K_v Channels in Microglia

In seeking to determine whether K_v channels regulate microglia activation, we first examined K_v channel expression in rat microglia by recording the whole-cell outward K^+ current induced by voltage steps (see Fig. 1). In one group of microglia cultures ($n = 9$), the average instantaneous outward K^+ current (an A-type-like outward current) density was 79.8 ± 6.3 pA/pF, and it was reduced to 46.7 ± 5.5 pA/pF when 4-AP was added to the bath. In another group of microglial cells ($n = 9$), the average steady-state K^+ current was 46.8 ± 10.4 pA/pF, and it was reduced to 33.9 ± 9.2 pA/pF when 5 mM TEA was introduced to the bath. Addition of 4-AP or TEA to the bath produced 41.5 ± 7.2% or 27.6 ± 8.9% reduction of outward K^+ current, respectively (see Fig. 1). To estimate K^+ current density, the capacitance of microglial cells was determined and used to obtain an estimate of cell surface area. The average whole-cell capacitance was 12.4 ± 3.0 pF, with a range of 5–27.5 pF ($n = 75$).

Enhancement of Microglia Outward K^+ Current by gp120

Following confirmation of K_v channel expression in microglia, we tested if gp120 could alter the outward K^+ current in microglia. Incubation of microglia with gp120 for 1–2 h enhanced whole cell outward K^+ current in a dose-dependent manner (see Fig. 2). When microglia were treated with gp120 at concentrations of 100, 200, and 400 pM, the average instantaneous outward K^+ cur-

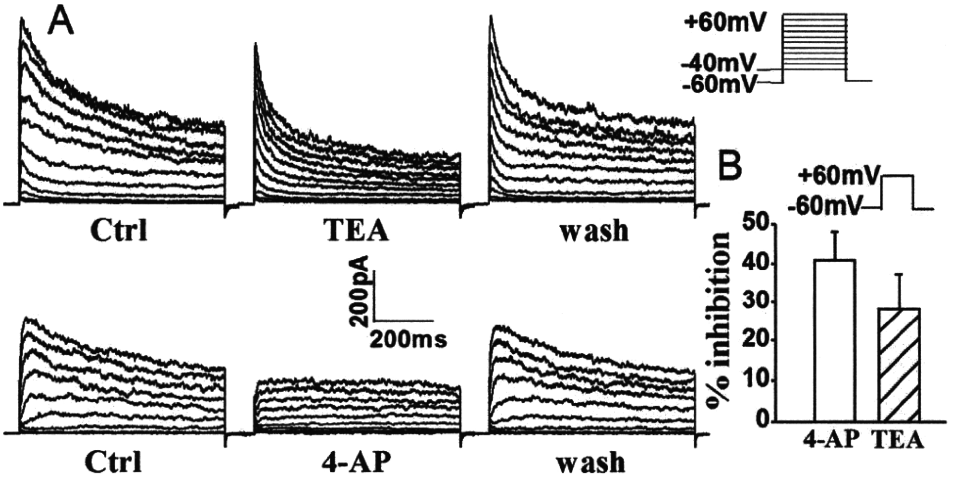

Fig. 1. Expression of outward K^+ current in rat microglia. Panel A shows examples illustrating the voltage-dependent outward K^+ current recorded in rat microglia and the partial blockade of outward K^+ current by TEA (upper) and 4-AP (lower). Panel B depicts the average inhibition of whole-cell outward K^+ current in microglia by 4-AP and TEA when measured at command voltage step of +60 mV. Bars represent mean ± SEM (the same in the following figures unless indicated). Voltage protocol employed to generate outward K^+ current is shown above Panel B.

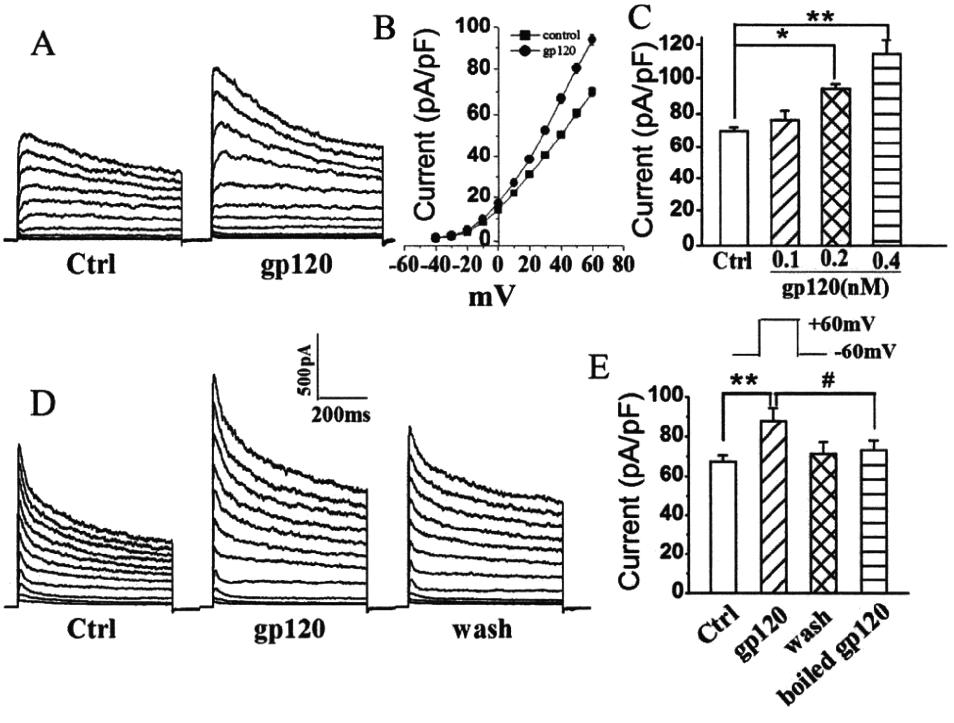

Fig. 2. gp120 enhances microglia whole-cell outward K^+ current in a dose-dependent manner. **A**: Typical outward K^+ currents recorded from a control and a gp120-treated microglia as indicated. **B**: I–V curves showing gp120 increases outward K^+ current. **C**: gp120 increases outward K^+ current in a dose-dependent manner. The graph plots mean outward K^+ current densities measured at +60 mV. **D**: Outward K^+ current recorded in microglia before (Ctrl), during (gp120), and after (wash) bath application of gp120 (200 pM). **E**: Average outward K^+ current densities recorded in microglia cells as shown in **D** (n = 5) and in another five microglia treated with heat (boiled)-inactivated gp120, illustrating gp120 specific enhancement of outward K^+ current. *, $P < 0.05$ vs. Ctrl; **, $P < 0.01$ vs. Ctrl; #, $P < 0.05$ vs. boiled gp120.

rent densities (pA/pF) were 76.1 ± 5.7 (n = 27), 94.0 ± 2.6 (n = 67), and 114.5 ± 8.4 (n = 11), respectively (see Fig. 2). In comparison with the average outward K^+ current density of 69.8 ± 2.1 pA/pF recorded in untreated (control) microglia (n = 46), the differences were statistically significant ($P < 0.05$), demonstrating an enhancement of whole cell outward K^+ current by gp120 in cultured rat microglia. Incubation of microglia with heat (boiled)-inactivated gp120 (200 pM) showed no significant effect on outward K^+ current density with an average of 73.3 ± 4.7 pA/pF (Fig. 2; n = 5), indicating a specific effect of gp120 on enhancing outward K^+ current in microglia.

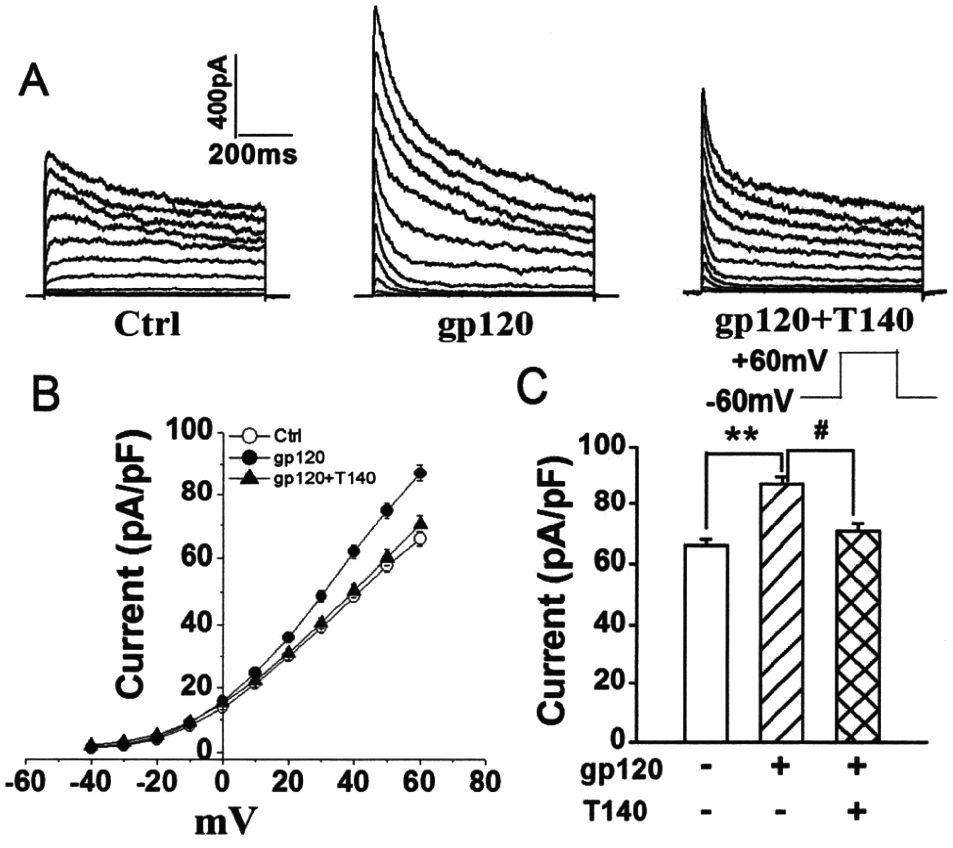

Fig. 3. Blockade of gp120-induced enhancement of microglial outward K^+ current by T140, a specific CXCR4 antagonist. **A**: Typical current traces recorded from control, gp120−, and gp120+T140-treated microglia as indicated. **B**: I–V curves of peak outward K^+ currents as shown in A. **C**: Bar graph showing the mean current densities (measured at +60 mV) recorded in control, gp120−, and gp120+T140-treated microglia. Note that gp120 enhanced outward K+ current and this enhancement was blocked by T140. ** $P < 0.01$ vs. ctrl; # $P < 0.05$ vs. gp120+T140.

Blockade of gp120-Induced Enhancement of Outward K^+ Current by T140

It is well-known that microglia express chemokine receptor CXCR4 (Albright et al., 1999; Lavi et al., 1997). To examine if the gp120-induced enhancement of outward K^+ current was mediated through CXCR4 (a co-receptor for HIV-1 infection), we tested the effects of T140, a highly selective CXCR4 receptor antagonist, on gp120-induced enhancement of outward K^+ current in another group of cultured microglia. While it *per se* had no significant effect on outward K^+ current when added to the bath, T140 (50 nM) significantly blocked gp120-induced enhancement of outward K^+ current recorded in microglia. The average instantaneous K^+ current densities without (control) and with addition of gp120 (200 pM) to the bath solution were 65.9 ± 2.2 pA/pF (n = 92) and 86.9 ± 2.7 pA/pF (n = 75), respectively. In contrast, the current density was 70.6 ± 2.5 pA/pF (n = 64) when both T140 and gp120 were added to the bath. In comparison with the K^+ current recorded when gp120 was added alone, the difference was statistically significant ($P < 0.05$), indicating that gp120 increases microglia outward K^+ current via CXCR4 (Fig. 3A,B).

Effect of gp120 on Microglia K_v Channel Biophysical Properties

To determine if gp120 alters microglia K_v channel biophysical properties, we examined the influence of gp120 on the properties of microglia K_v channel activation and steady-state inactivation. Figure 4A illustrates superimposed currents elicited by voltage steps applied in 10 mV increments from the holding potential −60 to +60 mV. Outward K^+ currents were first seen at −40 mV in gp120-treated microglia and became larger at stronger depolarizing command voltages. Normalized outward K^+ currents (Fig. 4A) were fitted to a Boltzmann equation: $G/G_{max} = 1/[1 + \exp(V - V_{1/2})/k]$, from which the voltage for half-maximal activation ($V_{1/2}$) and the slope factor (k) were calculated (Fig. 4C). Half-maximal activation occurred at 8.3 ± 0.9 mV and 12.9 ± 0.9 mV, with a slope factor, k, of 16.8 ± 0.9 mV and 15.2 ± 0.8mV for gp120-treated and control microglia, respectively (Fig. 4C; n = 21). The steady-state voltage dependence of inactivation of K^+ current was generated by varying the holding potential between −80 and +10 mV in 10 mV increments (Fig. 4B). After the holding potential was established for at least 1 min, cells

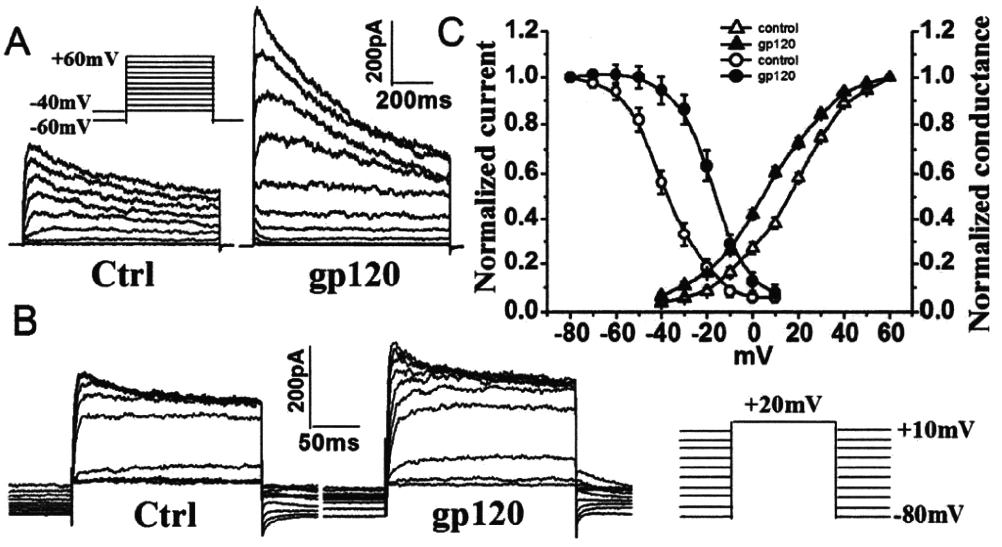

Fig. 4. Effects of gp120 on activation and inactivation of outward K^+ currents. **A**: Activation of outward K^+ current was induced using 700 ms voltage steps from a holding potential of −60 mV–40 mV at the first step, and then step to +60 mV in 10 mV increments. To ensure complete recovery from inactivation, successive voltage steps were separated by 5 s. **B**: Steady-state inactivation was measured by varying the holding potential (−80 – +10 mV) for 60 s at each voltage, then applying a 200 ms test pulse to +20 mV. **C**: Average of activation and inactivation curves. Note that gp120 shifted activation and inactivation to more negative potential and more negative potential, respectively.

were pulsed to a test potential of 20 mV for 200 ms. Steady-state inactivation began at approximately −70 mV and was complete at ~ 0 mV. Peak amplitudes of the evoked currents were measured, normalized, and then plotted as a function of the holding potential (Fig. 4B,C). The region under the intersection of activation and inactivation illustrates a window of tonic channel activity between −35 and 10 mV with maximal activity at the intersection voltage of −10 mV. Fitted with a Boltzmann function, half-maximal inactivation was at −15.4 ± 0.7 mV and −36.3 ± 0.8 mV, with k = 9.1 ± 0.7 mV and 10.1 ± 0.7 mV (n = 14) in gp120-treated and control microglia, respectively. In all cases, the voltage-dependent currents were highly K^+ selective because the reversal potential was very close to the calculated Nernst potential (−85 mV, data not shown) for K^+ concentrations used in this study (see Materials and Methods).

Involvement of PKA in gp120-Induced Increase of Outward K^+ Current

Protein phosphorylation can profoundly influence ion channel activity. Accumulating evidence indicate that K_v channels can be regulated by c-AMP-dependent protein kinase (PKA) (Chung and Schlichter, 1997; Fakler et al., 1994). We hypothesize that gp120 increases outward K^+ current via CXCR4 → PKA → K_v channel pathway. To test this hypothesis, we examined the effects of H89 (400 nM) on gp120 (200 pM)-induced enhancement of outward K^+ current in rat microglia. When applied alone, H89 failed to inhibit outward K^+ current (n = 28). In contrast, when co-applied with gp120, H89 inhibited the gp120-associated increase of outward K^+ current (see Fig. 5). The average outward K^+ current before (gp120) and after co-application of H89+gp120 were 86.2 ± 2.7 pA/pF (n = 75) and 69.1 ± 1.8 pA/pF (n = 42), respectively. The difference was statistically significant ($P < 0.05$), suggesting the involvement of PKA in gp120-induced increase of outward K^+ current.

Blockade of Microglia K_v Channels Inhibited Microglia-Induced Neuronal Injury

To examine biological significance of gp120-associated enhancement of outward K+ current, we studied neurotoxic activity of gp120-stimulated microglia and the protective effects of K_v channel blockers on microglia-induced neuronal injury. Rat microglia grown on the transwells were exposed to gp120 (200–500 pM) with or without K_v channel blockers (4-AP, 1 mM or TEA, 5 mM) for 24 h. After washing, the rat microglia were co-cultured with rat cortical neurons for additional 24 h and results showed that gp120-stimulated microglia induced apoptosis in 33.2 ± 3.9% of neurons examined (Fig. 6A,B). In comparison with the results of 4.7 ± 1.7% obtained in neurons co-cultured with non-stimulated microglia (control), the difference is statistically significant ($P < 0.01$), suggesting that gp120-stimulated microglia injure neurons. The injurious effect of microglia on neurons was confirmed by MTT assay (Fig. 6C). The neurotoxic effects of gp120-stimulated microglia were attenuated by K_v channel blockers (4-AP, TEA), CXCR4 receptor antagonist (T140), and PKA inhibitor (H89), respectively (see Fig. 6). As a positive control, LPS (0.5 μg/mL) was tested to stimulate microglia and the LPS-stimulated microglia, as anticipated, produced

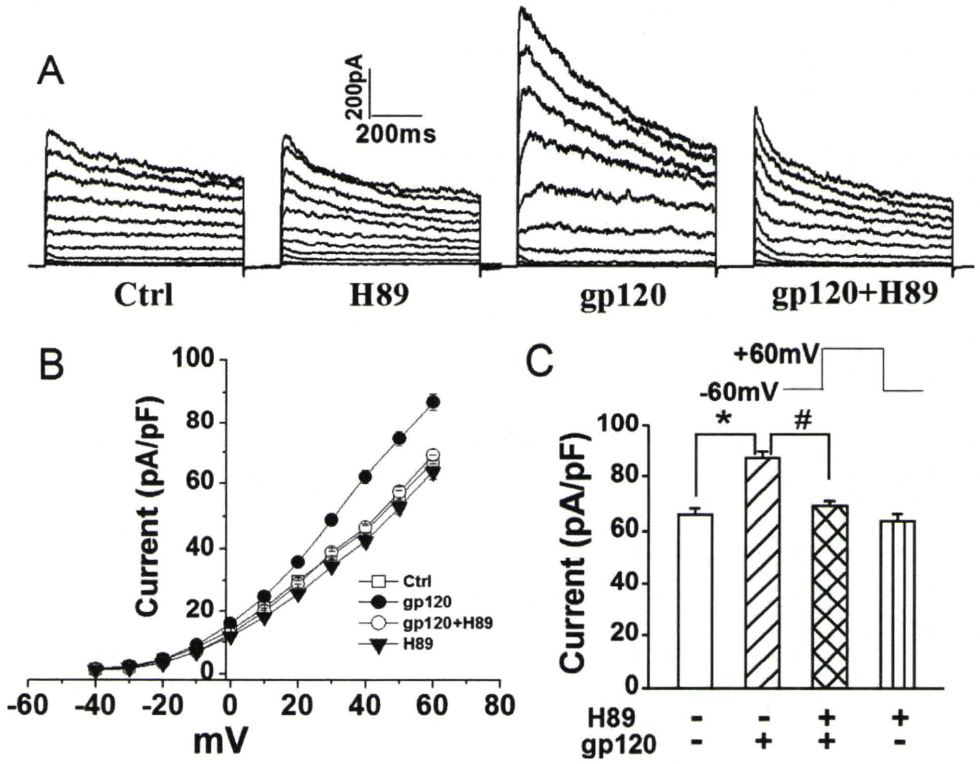

Fig. 5. Blockade of gp120-induced enhancement of outward K^+ currents by H89, a specific inhibitor for PKA. **A**: Representative current traces recorded from a control cell (Ctrl) and cells treated respectively with H89 alone, gp120 alone, and gp120+H89. The voltage protocol used to generate outward K^+ current was the same as the one shown in Fig. 1. **B**: I–V relationship illustrating the outward K^+ current densities as a function of voltage from the current traces shown in A. **C**: Summarized bar graphs showing average outward K^+ current densities measured at a voltage step +60 mV from microglia treated with H89 alone, gp120 alone, and gp120+H89. Note a significant blockade of gp120 enhancement of outward K^+ currents recorded in microglia. * $P < 0.05$ vs. ctrl, # $P < 0.05$ vs. gp120.

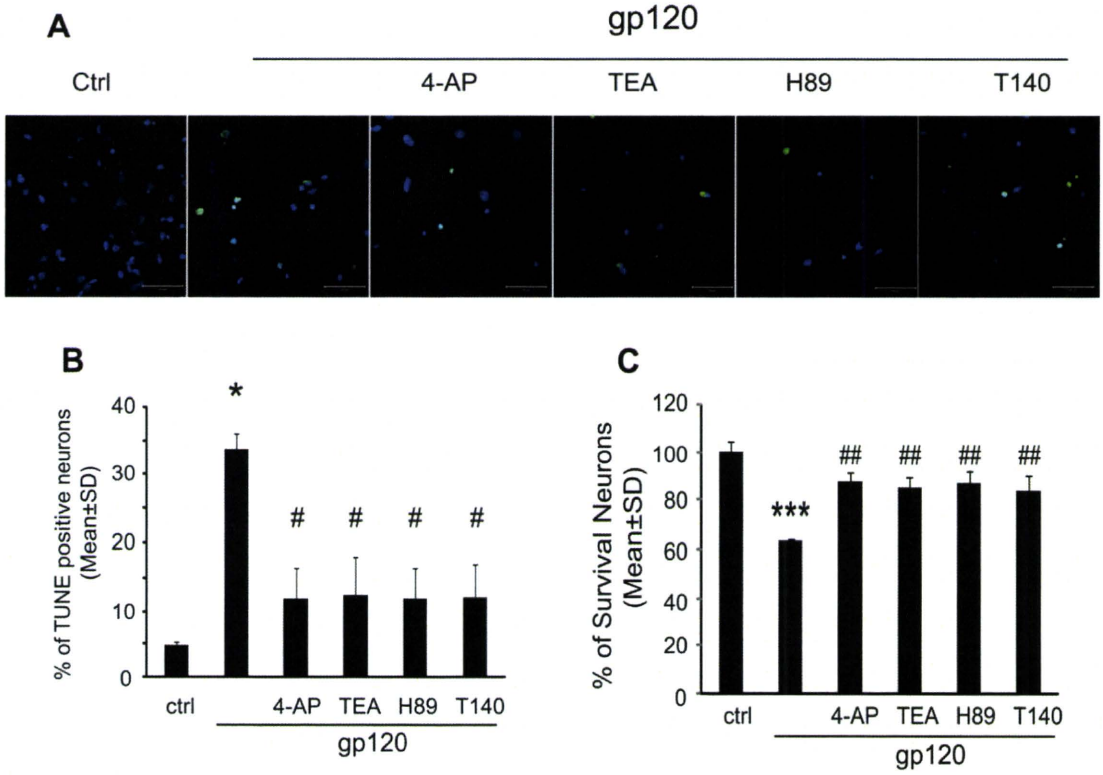

Fig. 6. Gp120-activated microglia produced cytotoxicity on neurons. Panel A: apoptotic neurons were visualized by TUNEL staining at ×400 original magnification (scale bar 50 μm). Panel B: Neuronal apoptosis was analyzed by combined TUNEL/DAPI staining and percentage of apoptotic neurons was determined by TUNEL-positive cells to normalize the total number of DAPI-positive cells. Compared with control group, an increasing percentage of apoptotic neurons were notably observed in gp120 treated group (Control vs. gp120, 7.7% vs. 33.77%). The apoptosis induced by gp120-stimulated microglia were attenuated by 4-AP, TEA, H89, and T140. Panel C: Neuronal viability was assessed by MTT assay. 4-AP, TEA, H89, and T140 significantly attenuated the neurotoxic activity of gp120-stimulated microglia. Values are expressed as mean ± SD of triplicate cultures. The results are representative of three independent experiments performed in triplicate determinations. *$P < 0.05$, ***$P < 0.001$ vs. Ctrl, # $P < 0.05$, ## $P < 0.01$ vs. gp120.

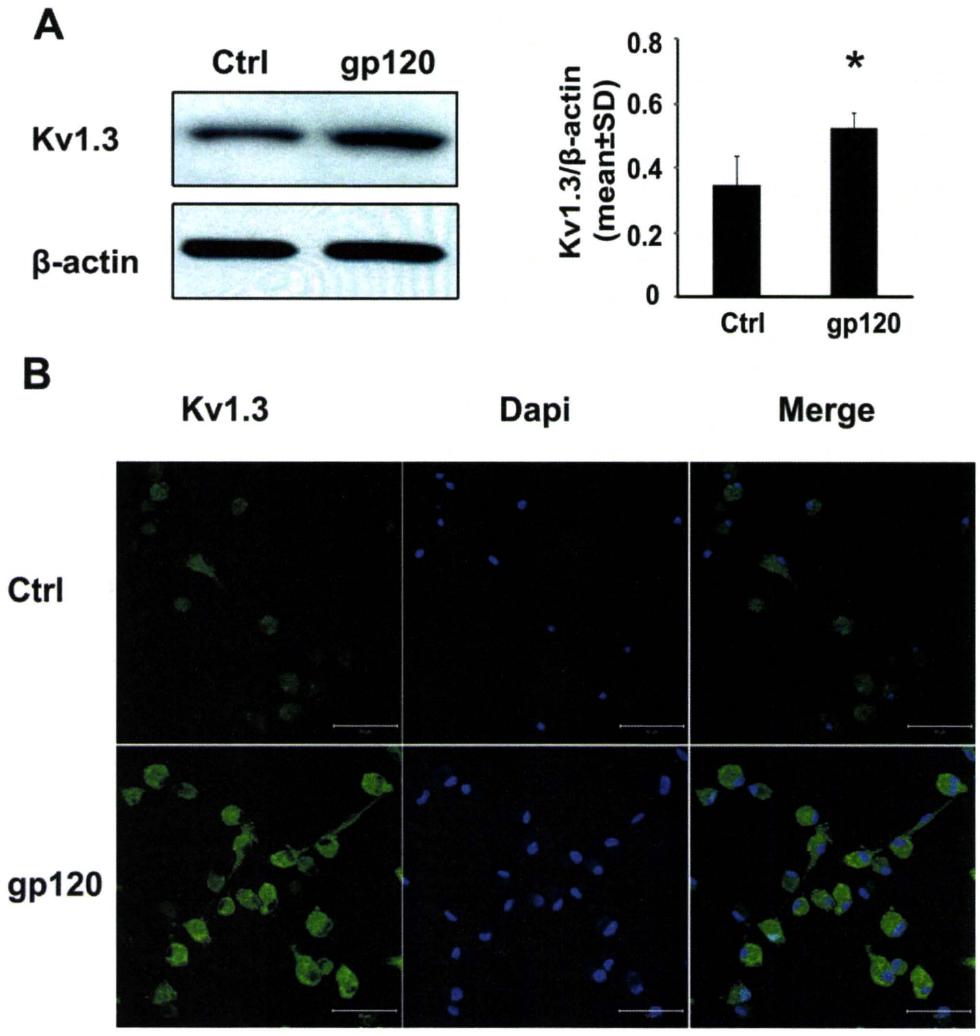

Fig. 7. gp120 enhanced expression levels of $K_v1.3$ in cultured microglia. Rat microglia (2×10^6 cells/well in 6 well plates or 0.5×10^6 cells/well in 24 well plates) were treated with or without gp120 (500 pM) for 24 h. The expression levels of $K_v1.3$ channel proteins were examined by Western blot and immunocytochemistry. Panel A: the representative scans showed Western blots for $K_v1.3$, and internal control β-actin (left). Each band density was normalized to its internal control and represents in bar graphs (right). Significant differences were detected in gp120 (1.5-fold increase) compared with nontreated microglia. $^*P < 0.05$ in comparison to control group were analyzed using Student's *t*-test. Panel B: Microglia were immunostained for expression of $K_v1.3$ (green). Images were visualized by fluorescent confocal microscopy at ×400 original magnification (scale bar 50 μm).

a significant neuronal apoptosis when co-cultured with neurons (data not shown).

Effects of gp120 on Microglia K_v Channel Expression

The voltage dependence of activation and inactivation of the outward K^+ current recorded in rat microglia, plus its blockade by 4-AP and TEA, suggest a possible identity of $K_v1.3$ current, which is in agreement with the up-regulated expression levels of $K_v1.3$ mRNA observed by other investigators (Eder, 1998; Norenberg et al., 1994; Schilling et al., 2000). To assess whether gp120 alters $K_v1.3$ protein expression, we examined the expression levels of $K_v1.3$ protein in microglia (2×10^6 cells/well, in six well plates) treated with or without gp120 for 24 h by western blot and immunocytochemistry. Our results showed that gp120 enhanced both the expression levels of $K_v1.3$ channel protein and immunofluorescent density of $K_v1.3$ staining in cultured microglia (see Fig. 7). The increase of $K_v1.3$ channel expression following gp120 treatment may underlie gp120-associated enhancement of outward K^+ current recorded in rat microglia.

Specific $K_v1.3$ Antagonist Blocks gp120-Induced Increase of Outward K^+ Current and Neuronal Apoptosis

After demonstration of gp120 enhancement of $K_v1.3$ expression, we further verified if the newly formed channels were functionally active and involved in gp120-associated increase of outward K^+ current and neuronal apoptosis using a specific $K_v1.3$ blocker margatoxin, MgTx, (Knaus et al., 1995). In another group of experiments, incubation of microglia with gp120 produced a signifi-

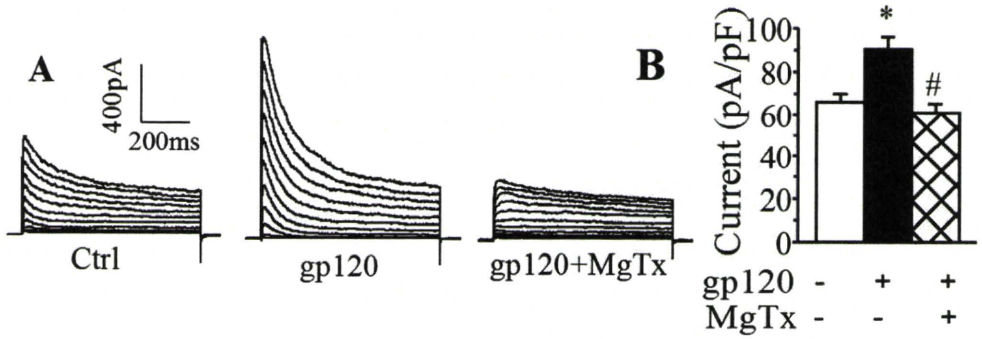

Fig. 8. Blockade of gp120 enhancement of outward K^+ current by MgTx, a specific $K_v1.3$ blocker. **A**: An example showing blockade of gp120-induced enhancement of outward K^+ current in rat microglia by MgTx. **B**: A summary bar graph illustrating MgTx significantly blocked gp120-induced enhancement of microglia outward K^+ current. Instantaneous outward K^+ current generated by a voltage step from −60 to +60 mV were measured and current densities were calculated. *, $P <$ 0.01 gp120-MgTx- vs. gp120+MgTx-; #, $P < 0.01$ gp120+MgTx- vs. gp120+MgTx+.

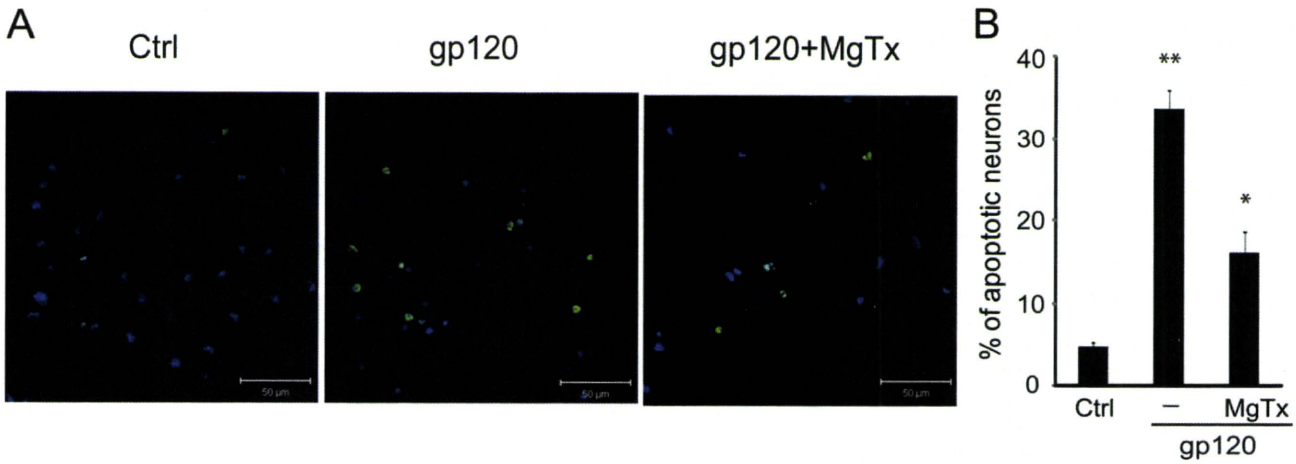

Fig. 9. Neurotoxic activity induced by gp120-stimulated microglia was blocked by MgTx in a microglia-neuronal co-culture system. **A**: Apoptotic neurons were assayed by TUNEL staining and visualized (green) via confocal microscopy at ×400 original magnifications. Scale bar equals 50 μM. **B**: Quantification of apoptotic neurons was made by enumeration of TUNEL-positive cells and expressed as percentage of total number of DAPI-positive cells counted. Note that gp120-stimulated microglia produced a significant increase of apoptotic neurons and the blockade of microglia $K_v1.3$ channel by MgTx significantly reduced microglia-induced neuronal apoptosis.

cant ($P < 0.01$) enhancement of outward K^+ current with an average current density of 90.4 ± 5.7 pA/pF (Fig. 8; $n = 12$) when compared with the current density (65.7 ± 4.3 pA/pF, $n = 10$) recorded in control (without gp120 treatment) microglia. Addition of MgTx (100 nM) to the bath solution abolished gp120-induced increase of outward K^+ current with an average of instantaneous current density of 60.5 ± 4.5 pA/pF (Fig. 8; $n = 8$). In comparison with the current density recorded in microglia treated with gp120, the difference was statistically significant ($P < 0.01$). The involvement of $K_v1.3$ in gp120-innduced neuronal injury was demonstrated by the results showing a significant attenuation of gp120-induced neuronal apoptosis by pretreatment of microglia with MgTx in microglia-neuronal co-culture system as shown in Fig. 9. These results indicate that the newly formed $K_v1.3$ channels were functional and involved in gp120-associated enhancement of outward K^+ current in rat microglia.

DISCUSSION

As the targets for HIV-1 infection and the producers of neurotoxins, microglia play an important role in the pathogenesis of HAND and other neurodegenerative disorders. It is widely accepted that the infected and immune-activated microglia secrete a variety of bioactive substances including viral protein gp120, resulting in neuronal dysfunction and death (Garden, 2002; Glass and Wesselingh, 2001). The mechanisms underlying microglia-associated neuropathogenesis are not fully understood. In this study, we demonstrated that HIV-1 gp120 increased the levels of $K_v1.3$ expression and enhanced outward K^+ current in cultured rat microglia via CXCR4-PKA signaling pathways. The enhancement of outward K^+ current was associated with microglia neurotoxicity evident through experimental results showing the blockade of microglia $K_v1.3$ channels suppressed microglia-associated neurotoxicity *in vitro*.

In HIV-1-infected brain, gp120, shed from virions and/or secreted from HIV-1-infected microglia/macrophages, has the potential to diffuse and interact directly with surrounding and distant neural cells through activation of CXCR4 receptors(Bachis and Mocchetti, 2004; Hesselgesser et al., 1998; Meucci et al., 1998), or by stimulation of uninfected microglia to release neurotoxins which act indirectly on local and distant neural cells, or both. Transgenic mice expressing gp120 manifest a spectrum of neuronal and glial changes resembling abnormalities in brains of HIV-1-infected humans and the severity of damage correlated positively with brain levels of gp120 expression (Toggas et al., 1994). While the precise mechanisms on how gp120 stimulates microglia production of neurotoxins remains to be determined, the enhancement of outward K^+ current by gp120 through CXCR4 may represent one of such potential mechanisms, as microglia-associated neurotoxicity was blocked either by a CXCR4 antagonist or by K_v channel blockers.

Microglia express a defined pattern of K_v channels, which is distinct from other glial cells and neurons. This pattern undergoes defined changes with microglia activation. It is believed that microglia K_v channels, albeit in a lower density than their excitable counterparts, play an important role in the switch from one functional state to another (Farber and Kettenmann, 2005; Kotecha and Schlichter, 1999). Patch clamp studies of microglia in cell cultures and in tissue slices have demonstrated that outward rectifier $K_v1.3$ and $K_v1.5$ are dominant K_v channels (Eder, 1998; Kotecha and Schlichter, 1999; Newell and Schlichter, 2005; Pannasch et al., 2006; Schilling et al., 2000). Our results showed that elevated levels of $K_v1.3$ expression and enhanced outward K^+ currents were detected in gp120-stimulated microglia and that the neuronal apoptosis induced by gp120-stimulated microglia was blocked by K_v channel blockers. These results suggest that gp120-induced elevation of K_v channel expression and enhancement of outward K^+ current might trigger microglia-associated neurotoxicity. Whereas the functional roles of $K_v1.3$ in microglia remain to be determined, evidence from this study and others indicates that the newly formed $K_v1.3$ channels appear to be involved in microglia activation and subsequent production of neurotoxins (Eder, 1998, 2005; Fordyce et al., 2005; Kotecha and Schlichter, 1999).

Ion channels are the targets of many intracellular signaling pathways including protein phosphorylation. These processes can modify channel activity and alter cellular electrophysiological properties. Thus, protein phosphorylation is an important physiological regulator of K_v channel function. Amino acid sequences of $K_v1.3$ clones from mouse, rats and human are very similar, with >98% homology between human and rat clones (Chandy and Gutman, 1995). All $K_v1.3$ clones contain several potential PKA and PKC phosphorylation sites, with one strong PKA site at the COOH terminus (Kennelly and Krebs, 1991). Evidence that $K_v1.3$ channels can be regulated by PKA includes reports of enhancement of delayed rectifier K^+ currents in vascular smooth muscle cells (Aiello et al., 1995), squid giant axon (Perozo et al., 1989) and human T lymphocytes (Chung and Schlichter, 1997). Inhibition of serine/threonine protein phosphatases with okadaic acid increases $K_v1.3$ current and shifts the voltage dependence of activation and inactivation to more positive potentials. Inhibition of PKA by a specific PKA inhibitor decreases $K_v1.3$ current. These observations indicate that $K_v1.3$ activity can be regulated by serine/threonine phosphorylation. The results obtained in this study revealed that the gp120-induced enhancement of microglia outward K^+ current was blocked by a specific PKA inhibitor H89, suggesting that activation of CXCR4 by gp120 in microglia causes cAMP-dependent PKA activation, resulting in $K_v1.3$ phosphorylation and consequent enhancement of channel activity.

$K_v1.3$ is predominantly expressed in immunocytes including microglia, lymphocytes, and macrophages and is important for immunocyte-mediated immune and inflammatory responses (Beeton et al., 2006; Chandy et al., 2004). Mounting evidence suggests that immune and inflammatory responses mediated by the activated microglia, the predominant resident CNS cell type productively infected by HIV-1(Lipton and Gendelman, 1995), play a pivotal role in the pathogenesis of HAND (Dheen et al., 2007; Garden, 2002; Glass and Wesselingh, 2001). Thus, studies on identification of specific target(s) to regulate microglia activation and resultant production of neurotoxins are highly imperative. Our results, gp120-associated neurotoxicity was blocked by a specific $K_v1.3$ blocker MgTx, indicate that $K_v1.3$ expressed in microglia may function as a potential target for the development of therapeutic strategies for HAND and perhaps for other neurodegenerative disorders. We anticipate that blockade of $K_v1.3$ channels in microglia might attenuate microglia-associated neurotoxicity, resulting in the protection of neurons from HIV-associated challenge in the infected brain. It is worth pointing out that there may be side effects by systemic or intracranial administration of $K_v1.3$ blockers since small amounts of $K_v1.3$ are also expressed in several brain regions such as hippocampus, and pyriform cortex (Kues and Wunder, 1992). However, such potential side effects might be minimal as animals deficient in $K_v1.3$ exhibited only a heightened sense of smell and distinct structure alterations in the olfactory bulb (Fadool et al., 2004). Thus, the potential for development of specific $K_v1.3$ blockers to suppress microglia-associated neurotoxicity is optimistic.

In summary, the experimental data provide *in vitro* evidence that HIV-1gp120 enhances outward K^+ current in cultured rat microglia via CXCR4 → cAMP-dependent PKA signaling pathway. Gp120 elevates the levels of K_v channel expression and alters K_v channel biophysical properties. Biological significance of gp120 enhancement of microglia outward K^+ current was demonstrated by experimental results that blockade of microglia K_v channels by K_v channel blockers suppresses microglia-induced neurotoxicity. As such, the K_v channel

expressed in microglia may function as a potential target in the development of therapeutic strategies for neurodegenerative disorders by which the activated resident microglia play a critical role in the pathogenesis.

ACKNOWLEDGMENTS

The authors thank Mr. Bryan Katafiasz for reading the manuscript. The authors extend special thanks to Ms. Julie Ditter, Ms. Robin Taylor, and Ms. Johna Belling for their excellent administrative supports and to two anonymous reviewers for their critical criticisms and helpful comments.

REFERENCES

Aiello EA, Walsh MP, Cole WC. 1995. Phosphorylation by protein kinase A enhances delayed rectifier K+ current in rabbit vascular smooth muscle cells. Am J Physiol 268:H926–H934.

Albright AV, Shieh JT, Itoh T, Lee B, Pleasure D, O'Connor MJ, Doms RW, Gonzalez-Scarano F. 1999. Microglia express CCR5, CXCR4, and CCR3, but of these, CCR5 is the principal coreceptor for human immunodeficiency virus type 1 dementia isolates. J Virol 73:205–213.

Bachis A, Mocchetti I. 2004. The chemokine receptor CXCR4 and not the N-methyl-D-aspartate receptor mediates gp120 neurotoxicity in cerebellar granule cells. J Neurosci Res 75:75–82.

Beeton C, Wulff H, Standifer NE, Azam P, Mullen KM, Pennington MW, Kolski-Andreaco A, Wei E, Grino A, Counts DR, others. 2006. Kv1.3 channels are a therapeutic target for T cell-mediated autoimmune diseases. Proc Natl Acad Sci U S A 103:17414–17419.

Chandy KG, Gutman GA. 1995. Voltage-gated potassium channel genes. In: North RA, editor. Ligand and Voltage-gated Ion Channels. Bpca Raton, FL: CRC. pp 1–71.

Chandy KG, Wulff H, Beeton C, Pennington M, Gutman GA, Cahalan MD. 2004. K+ channels as targets for specific immunomodulation. Trends Pharmacol Sci 25:280–289.

Chung I, Schlichter LC. 1997. Regulation of native Kv1.3 channels by cAMP-dependent protein phosphorylation. Am J Physiol 273:C622–C633.

Dheen ST, Kaur C, Ling EA. 2007. Microglial activation and its implications in the brain diseases. Curr Med Chem 14:1189–1197.

Eder C. 1998. Ion channels in microglia (brain macrophages). Am J Physiol 275:C327–C342.

Eder C. 2005. Regulation of microglial behavior by ion channel activity. J Neurosci Res 81:314–321.

Eder C, Fischer HG, Hadding U, Heinemann U. 1995. Properties of voltage-gated currents of microglia developed using macrophage colony-stimulating factor. Pflugers Arch 430:526–533.

Elkabes S, Peng L, Black IB. 1998. Lipopolysaccharide differentially regulates microglial trk receptor and neurotrophin expression. J Neurosci Res 54:117–122.

Fadool DA, Tucker K, Perkins R, Fasciani G, Thompson RN, Parsons AD, Overton JM, Koni PA, Flavell RA, Kaczmarek LK. 2004. Kv1.3 channel gene-targeted deletion produces "Super-Smeller Mice" with altered glomeruli, interacting scaffolding proteins, and biophysics. Neuron 41:389–404.

Fakler B, Brandle U, Glowatzki E, Zenner HP, Ruppersberg JP. 1994. Kir2.1 inward rectifier K+ channels are regulated independently by protein kinases and ATP hydrolysis. Neuron 13:1413–1420.

Farber K, Kettenmann H. 2005. Physiology of microglial cells. Brain Res Brain Res Rev 48:133–143.

Fischer HG, Eder C, Hadding U, Heinemann U. 1995. Cytokine-dependent K+ channel profile of microglia at immunologically defined functional states. Neuroscience 64:183–191.

Fordyce CB, Jagasia R, Zhu X, Schlichter LC. 2005. Microglia Kv1.3 channels contribute to their ability to kill neurons. J Neurosci 25: 7139–7149.

Garden GA. 2002. Microglia in human immunodeficiency virus-associated neurodegeneration. Glia 40:240–251.

Gendelman HE, Eiden L, Epstein L, Grant I, Lipton SA, McArthur JC, Pomerantz R, Price R, Swindells S. 1997. Neuropathogenesis of HIV-1 Dementia: A Panel Discussion. New York: Chapman & Hall.

Genis P, Jett M, Bernton EW, Boyle T, Gelbard HA, Dzenko K, Keane RW, Resnick L, Mizrachi Y, Volsky DJ, others. 1992. Cytokines and arachidonic metabolites produced during human immunodeficiency virus (HIV)-infected macrophage-astroglia interactions: implications for the neuropathogenesis of HIV disease. J Exp Med 176:1703–1718.

Glass JD, Wesselingh SL. 2001. Microglia in HIV-associated neurological diseases. Microsc Res Tech 54:95–105.

Hesselgesser J, Taub D, Baskar P, Greenberg M, Hoxie J, Kolson DL, Horuk R. 1998. Neuronal apoptosis induced by HIV-1 gp120 and the chemokine SDF-1 alpha is mediated by the chemokine receptor CXCR4. Curr Biol 8:595–598.

Kaul M, Garden GA, Lipton SA. 2001. Pathways to neuronal injury and apoptosis in HIV-associated dementia. Nature 410:988–994.

Kennelly PJ, Krebs EG. 1991. Consensus sequences as substrate specificity determinants for protein kinases and protein phosphatases. J Biol Chem 266:15555–15558.

Kielian T. 2004. Microglia and chemokines in infectious diseases of the nervous system: Views and reviews. Front Biosci 9:732–750.

Knaus HG, Koch RO, Eberhart A, Kaczorowski GJ, Garcia ML, Slaughter RS. 1995. [125I]margatoxin, an extraordinarily high affinity ligand for voltage-gated potassium channels in mammalian brain. Biochemistry 34:13627–13634.

Koenig S, Gendelman HE, Orenstein JM, Dal Canto MC, Pezeshkpour GH, Yungbluth M, Janotta F, Aksamit A, Martin MA, Fauci AS. 1986. Detection of AIDS virus in macrophages in brain tissue from AIDS patients with encephalopathy. Science 233:1089–1093.

Kotecha SA, Schlichter LC. 1999. A Kv1.5 to Kv1.3 switch in endogenous hippocampal microglia and a role in proliferation. J Neurosci 19:10680–10693.

Kues WA, Wunder F. 1992. Heterogeneous Expression Patterns of Mammalian Potassium Channel Genes in Developing and Adult Rat Brain. Eur J Neurosci 4:1296–1308.

Lavi E, Strizki JM, Ulrich AM, Zhang W, Fu L, Wang Q, O'Connor M, Hoxie JA, Gonzalez-Scarano F. 1997. CXCR-4 (Fusin), a co-receptor for the type 1 human immunodeficiency virus (HIV-1), is expressed in the human brain in a variety of cell types, including microglia and neurons. Am J Pathol 151:1035–1042.

Lipton SA, Gendelman HE. 1995. Seminars in medicine of the Beth Israel Hospital, Boston Dementia associated with the acquired immunodeficiency syndrome [see comments]. N Engl J Med 332:934–940.

Menteyne A, Levavasseur F, Audinat E, Avignone E. 2009. Predominant functional expression of Kv1.3 by activated microglia of the hippocampus after Status epilepticus. PLoS One 4:e6770

Meucci O, Fatatis A, Simen AA, Bushell TJ, Gray PW, Miller RJ. 1998. Chemokines regulate hippocampal neuronal signaling and gp120 neurotoxicity. Proc Natl Acad Sci U S A 95:14500–14505.

Miwa T, Furukawa S, Nakajima K, Furukawa Y, Kohsaka S. 1997. Lipopolysaccharide enhances synthesis of brain-derived neurotrophic factor in cultured rat microglia. J Neurosci Res 50:1023–1029.

Newell EW, Schlichter LC. 2005. Integration of K+ and Cl- currents regulate steady-state and dynamic membrane potentials in cultured rat microglia. J Physiol 567:869–890.

Norenberg W, Gebicke-Haerter PJ, Illes P. 1994. Voltage-dependent potassium channels in activated rat microglia. J Physiol 475:15–32.

Pannasch U, Farber K, Nolte C, Blonski M, Yan Chiu S, Messing A, Kettenmann H. 2006. The potassium channels Kv1.5 and Kv1.3 modulate distinct functions of microglia. Mol Cell Neurosci 33:401–411.

Perozo E, Bezanilla F, Dipolo R. 1989. Modulation of K channels in dialyzed squid axons. ATP-mediated phosphorylation. J Gen Physiol 93: 1195–1218.

Schilling T, Quandt FN, Cherny VV, Zhou W, Heinemann U, Decoursey TE, Eder C. 2000. Upregulation of Kv1.3 K(+) channels in microglia deactivated by TGF-beta. Am J Physiol Cell Physiol 279:C1123–C1134.

Toggas SM, Masliah E, Rockenstein EM, Rall GF, Abraham CR, Mucke L. 1994. Central nervous system damage produced by expression of the HIV-1 coat protein gp120 in transgenic mice. Nature 367:188–193.

Walz W, Bekar LK. 2001. Ion channels in cultured microglia. Microsc Res Tech 54:26–33.

Bioorganic & Medicinal Chemistry 19 (2011) 3216–3220

Contents lists available at ScienceDirect

Bioorganic & Medicinal Chemistry

journal homepage: www.elsevier.com/locate/bmc

Concise site-specific synthesis of DTPA–peptide conjugates: Application to imaging probes for the chemokine receptor CXCR4

Ryo Masuda, Shinya Oishi *, Hiroaki Ohno, Hiroyuki Kimura, Hideo Saji, Nobutaka Fujii *

Graduate School of Pharmaceutical Sciences, Kyoto University, Sakyo-ku, Kyoto 606-8501, Japan

ARTICLE INFO

Article history:
Received 17 February 2011
Revised 25 March 2011
Accepted 26 March 2011
Available online 2 April 2011

Keywords:
CXCR4
DTPA
Molecular imaging

ABSTRACT

Diethylenetriaminepentaacetic acid (DTPA) is a useful chelating agent for radionuclides such as ^{68}Ga, ^{99m}Tc and ^{111}In, which are applicable to nuclear medicine imaging. In this study, we established a facile synthetic protocol for the production of mono-DTPA-conjugated peptide probes. A novel monoreactive DTPA precursor reagent was synthesized in two steps using the chemistry of the *o*-nitrobenzenesulfonyl (Ns) protecting group, and under mild conditions this DTPA precursor was incorporated onto an N^{ε}-bromoacetylated Lys of a protected peptide resin. The site-specific DTPA conjugation was facilitated by using a highly acid-labile 4-methyltrityl (Mtt) protecting group for the target site of the bioactive peptide during the solid-phase synthesis. A combination of both techniques yielded peptides with disulfide bonds, such as octreotide and polyphemusin II-derived CXCR4 antagonists. DTPA–peptide conjugates were purified in a single step following cleavage from the resin and disulfide bond formation. This site-specific on-resin construction strategy was used for the design and synthesis of a novel In-DTPA-labeled CXCR4 antagonist, which exhibited highly potent inhibitory activity against SDF-1–CXCR4 binding.

1. Introduction

Recent progress in molecular imaging methodologies such as positron emission tomography (PET), single-photon emission computed tomography (SPECT) and optical imaging technologies has significantly improved the early detection and diagnosis of malignant tumors. To visualize the specific molecular events involved in the physiological and/or pathological processes, a number of peptide-based imaging probes have been developed for overexpressed receptors of peptide hormones and extracellular matrix proteins.[1] These probes are usually designed by a combination of three components: a target-specific vector peptide, an imaging part such as a radionuclide or fluorophore, and a linker to covalently or noncovalently conjugate the peptide with the imaging moiety. The addition of a functional moiety onto small-sized bioactive peptides may be highly susceptible to interaction with receptors or counterpart molecules. Consequently, there have been many reagents of choice for appropriate protein/peptide modifications. In addition, to determine the best labeling position from structure-function relationship studies, versatile synthetic approaches toward various types of labeled peptide are desired.

Polyamino polycarboxylate ligands efficiently coordinate metal radioisotopes to aid the radiolabeling of bioactive peptides. Among the chelating ligands, 1,4,7,10-tetraazacyclododecane-1,4,7,10-tetraacetic acid (DOTA) **1a** has been most widely utilized, since a variety of metal radioisotopes for both diagnostic and therapeutic purposes form complexes with high affinity and kinetic stability (Fig. 1).[2] DOTA-modification of bioactive peptides is facilitated by commercially available reagents such as DOTA-NHS **1b** and DOTA-maleimide **1c** to provide the expected peptides in a single step.[3,4] Alternatively, tris(*tert*-butyl)-DOTA **2a** with a free carboxyl group is employed for the modification of an amino group of protected peptides bound to solid-supports.[5] Lysine or phenylalanine derivatives **2b,c** possessing a *tert*-butyl-protected DOTA moiety are also useful components for the peptide sequence assembly.[6] *tert*-Butyl protecting groups in these reagents are easily removed during the final side-chain deprotection process of peptide synthesis.

In contrast to these DOTA derivatives, there has been limited work exploring the application of the diethylenetriaminepentaacetic acid (DTPA) chelating group **3a**, although DTPA represents a promising alternative, especially for ^{68}Ga, ^{99m}Tc and ^{111}In (Fig. 1). The recent success of DTPA-based probes is exemplified by a glucagon-like peptide-1 (GLP-1) receptor ligand, [Lys^{40}(Ahx-DTPA-^{111}In)NH_2]-exendin-4, for insulinoma diagnosis.[7] The DTPA group also works as a more favorable functional group than DOTA to facilitate the biological or biodistribution properties of several probes.[8] For the preparation of DTPA-conjugated imaging probes, several conjugation reagents have been developed. The most familiar cyclic diethylenetriaminepentaacetic dianhydride **4**

* Corresponding authors. Tel.: +81 75 753 4551; fax: +81 75 753 4570.
E-mail addresses: soishi@pharm.kyoto-u.ac.jp (S. Oishi), nfujii@pharm.kyoto-u.ac.jp (N. Fujii).

0968-0896/$ - see front matter © 2011 Elsevier Ltd. All rights reserved.
doi:10.1016/j.bmc.2011.03.059

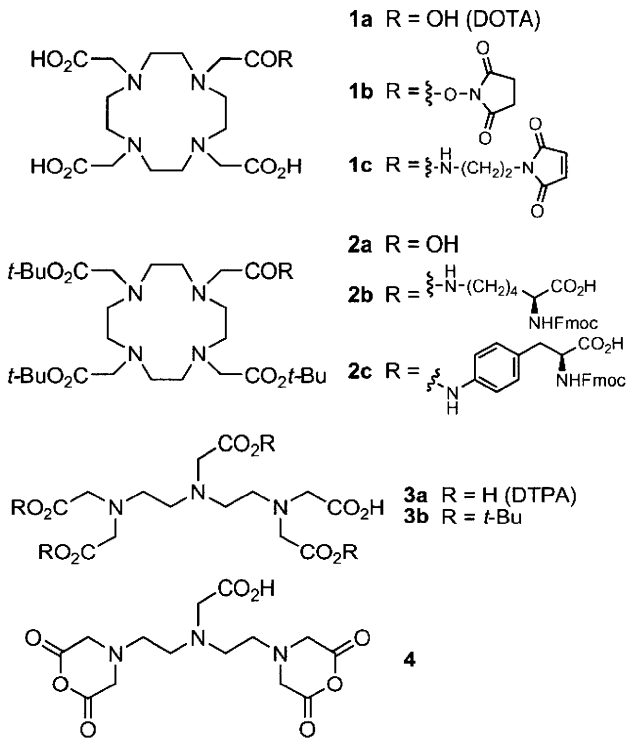

Figure 1. Structures of radionuclide chelating agents and the precursors.

is a bifunctional chelating agent, which can conjugate with peptide hormones and antibodies.[9] Using this reagent, concomitant formations of a bis-conjugated product[10] and intra- and intermolecular cross-linked products[11] were unavoidable. Monoreactive DTPA derivatives have also been developed for the preparation of DTPA–peptide conjugates without the unfavorable by-product formations.[12,13] For example, we reported the synthesis and application of 3,6,9,9-tetrakis[(*tert*-butoxycarbonyl)methyl]-3,6,9-triazanonanoic acid **3b** (mDTPA),[14] in which the four carboxylates were protected with *tert*-butyl ester. However, a longer process from the commercially available reagents is required for the synthesis of these DTPA-conjugation reagents (Scheme 1A).

Accordingly, to establish a facile and efficient synthetic method for DTPA–peptide conjugates, we have investigated the site-specific and on-resin construction of a DTPA moiety. Herein, we describe the short-step synthesis of a DTPA precursor using the *o*-nitrobenzenesulfonyl (Ns) protecting group and the solid-phase synthesis of DTPA–peptide conjugates. The design and synthesis of DTPA–peptide conjugates that potentially target the somatostatin receptor and chemokine receptor CXCR4 are also presented.[15]

2. Results and discussion

2.1. Synthesis of a DTPA-conjugation reagent and the application to octreotide derivatives

The synthetic scheme for the production of mDTPA reagent **10**, as described in our previous study, is presented in Scheme 1A. We hypothesized that two remedies could significantly improve the overall synthetic process of DTPA–peptide conjugates. First, the use of an Ns group in place of the trifluoroacetyl group was expected to serve as a temporary protecting group and an auxiliary group for global modification with four *tert*-butoxycarbonylmethyl groups. This potentially improves the stepwise synthesis of the intermediate **7** in the solution-phase. In addition, a secondary amine **8** as a nucleophilic precursor for the bromoacetyl group on peptide resin **11** can directly produce the overall DTPA framework of **12** on the solid support without the additional three-step modification process of **8** in solution (Scheme 1B).[16]

Synthesis of DTPA precursor **8** began with mono-Ns protection of the commercially available diethylenetriamine **5** (Scheme 2). The Ns-protected intermediate was successively treated with excess equivalent of *t*-butyl bromoacetate in a one-pot process. Although the solvent EtOH has been reported to be effective in predominantly giving the mono-Ns product,[17] concomitant production of bis-Ns product **14b** was not suppressed as in DMF. The treatment of excess diethylenetriamine **5** with NsCl in EtOH provided mono-Ns product **14a** in 65% yield (calculated based on NsCl), which can be readily purified by chromatography. Compound **14a** was then subjected to deprotection with mercaptoacetic acid and LiOH to provide the expected precursor **8** in 77% yield.

Using the resulting reagent **8**, DTPA-conjugation of [D-Phe^1]octreotide was investigated as a model study (Scheme 3), which is employed as a radionuclide imaging probe for the somatostatin receptor.[14,18,19] After peptide-chain elongation by Fmoc-based solid-phase peptide synthesis, the N-terminus of **16** was modified with bromoacetic acid and 1,3-diisopropylcarbodiimide (DIC). Subsequently, the bromide **17** was treated with the reagent **8** in the presence of $(i\text{-Pr})_2$NEt to provide the fully protected peptide resin **18a**. Cleavage from the resin **18a** and disulfide formation under air-oxidation conditions provided [DTPA-D-Phe^1]octreotide **19a** with high purity. The bromoacetylated peptide **17** was also modified with commercially available DOTA precursor reagent **20**, using the identical procedure to provide [DOTA-D-Phe^1]octreotide **19b**.[20] These suggest that this on-resin modification procedure is widely applicable to any chelating reagents with nucleophilic functional groups such as DTPA and DOTA precursors.

2.2. Site-specific DTPA-conjugation of bioactive peptides: synthesis of CXCR4 receptor probes

It has been reported that a high level of CXCR4 expression in tumors is associated with malignant and metastatic properties.[21] Intrinsic SDF-1 release from the potential distal metastatic sites mediates organ-specific metastasis of CXCR4-expressing cells from the primary lesions. Since CXCR4-expressing cancer stem cells are related to the metastatic spread in orthotopic primary tumors,[22] it is of considerable importance to develop potent CXCR4-imaging probes to detect potential cancer stem cells within malignant tumors, as exemplified by the diagnosis of bladder cancer by a fluorescent CXCR4 probe.[23,24]

Previously, we reported a DTPA-conjugated CXCR4 antagonist, DTPA-Ac-TZ14011 **26a**,[25] which was designed from a horseshoe crab-derived anti-HIV peptide T140. This peptide has β-sheet-like structures maintained by a disulfide bond, around which the pharmacophore residues for bioactivity are located.[26] For the site-specific conjugation at D-Lys^8 in the type II' β-turn region of T140 with a single DTPA group in the solution-phase, a secondary lysine (Lys^7) was substituted with arginine, which cannot be acylated by standard reagents.[25] Although a DTPA group was successfully ligated with maintenance of highly potent CXCR4 antagonistic activity in this case,[25] the accompanying substitutions needed for specific modification of other peptides may possibly lead to a decrease in the bioactivity. Therefore, we planned the facile site-specific DTPA conjugation on a solid-support for production of CXCR4 imaging probes without substitution of the secondary Lys^7 residue. To distinguish D-Lys^8 to be labeled in peptides **26**, the highly acid-labile 4-methyltrityl (Mtt) group was exploited for temporary protection of the ε-amino group during solid-phase peptide synthesis.[27] For the other Lys residues such as Lys^7 of

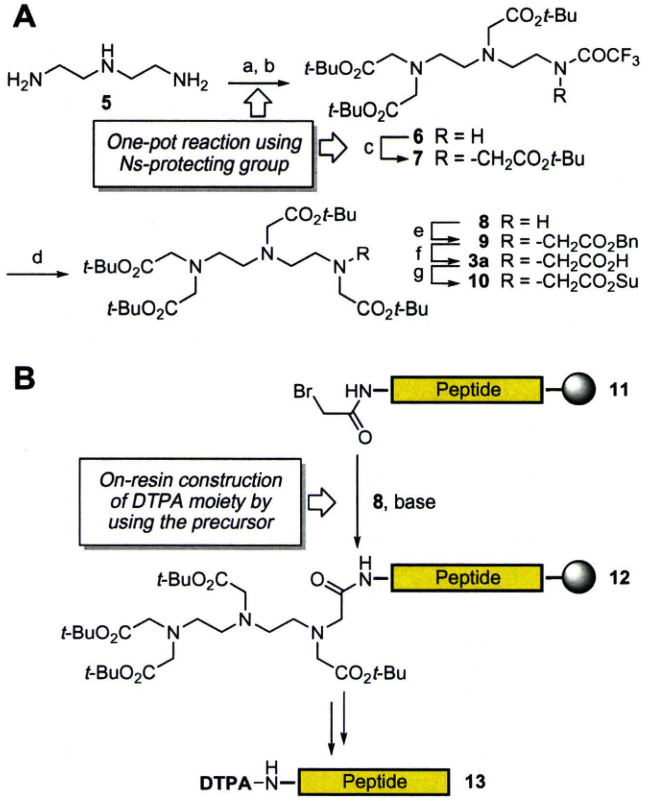

Scheme 1. (A) Synthetic scheme for the DTPA-conjugation reagent **10** prepared in our previous study; (B) synthetic plan for the DTPA-conjugated peptides in this study. Reagents: (a) CF_3CO_2Et; (b) $BrCH_2CO_2t$-Bu, $(i\text{-}Pr)_2NEt$; (c) $BrCH_2CO_2t$-Bu, NaH; (d) NH_2NH_2, *t*-BuOH; (e) $BrCH_2CO_2Bn$, $(i\text{-}Pr)_2NEt$; (f) H_2, Pd/C; (g) DCC, HOSu.

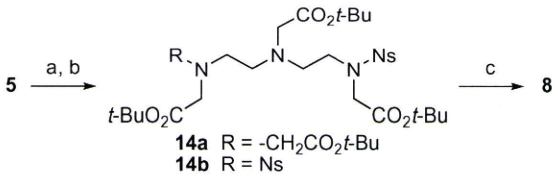

Scheme 2. Synthesis of DTPA precursor **8** via a global N-alkylation process using a Ns-protecting group. Reagents: (a) NsCl; (b) $BrCH_2CO_2t$-Bu, K_2CO_3; (c) $HSCH_2CO_2H$, LiOH.

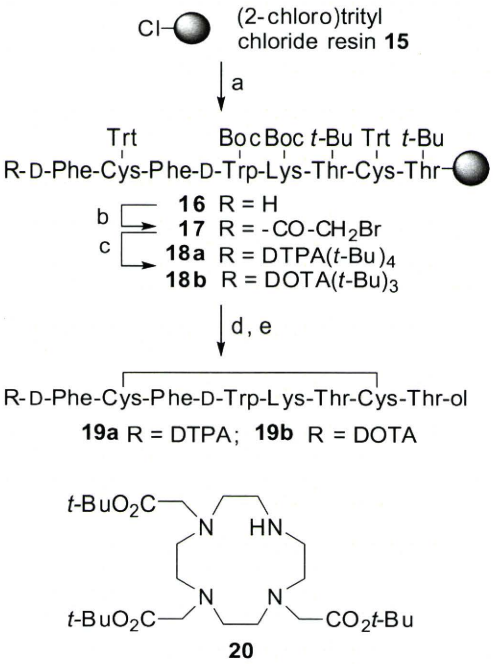

Scheme 3. Synthesis of DTPA- and DOTA-conjugated D-Phe-octreotides. Reagents: (a) Fmoc-based peptide synthesis; (b) $BrCH_2CO_2H$, DIC; (c) **8** for **18a**, or **20** for **18b**, $(i\text{-}Pr)_2NEt$ (d) TFA/H_2O/1,2-ethanedithiol (EDT) (95:2.5:2.5) for **19a**, 1 M TMSBr, thioanisole/TFA, 1,2-ethanedithiol, *m*-cresol for **19b**; (e) NH_4OH (air oxidation).

26b,c, a Boc group was employed. This group can be cleaved by the standard TFA-based treatment in Fmoc chemistry (Scheme 4). After the construction of the protected peptide resin, the orthogonal Mtt group at the labeling position was cleaved off using 1,1,1,3,3,3-hexafluoropropan-2-ol (HFIP). The resulting ε-amino group was successively modified with bromoacetic acid followed by the reagent **8** to provide the fully protected DTPA–peptide resin **25**. Final deprotection, air-oxidation and HPLC purification afforded the expected DTPA-conjugated CXCR4 antagonists **26a,b**. This concise protocol facilitates the selection of chelating structure and position(s) on the peptide chain, and aids structure–activity relationship studies aimed at exploring the more potent peptide probes. For example, a 4-fluorobenzoyl modification at the N-terminus, which should increase CXCR4 antagonism,[28] was easily appended to the peptide using this protocol to give the modified peptide **26c**. The subsequent treatment with nonradioactive $InCl_3$ in acidic conditions provided the In-DTPA-labeled CXCR4 antagonists **27a–c**.

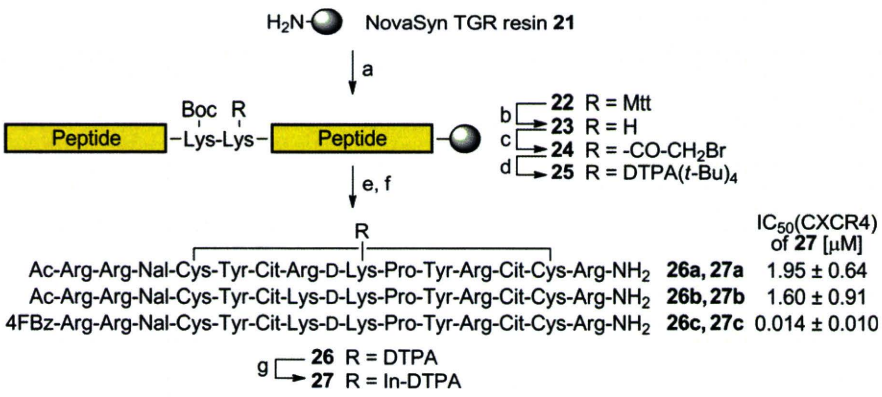

Scheme 4. Site-specific In-DTPA labeling of CXCR4 antagonists and biological activity. Reagents: (a) Fmoc-based peptide synthesis; (b) CH_2Cl_2/1,1,1,3,3,3-hexafluoro-2-propanol (HFIP)/2,2,2-trifluoroethanol (TFE)/triethylsilane (TES) (65:20:10:5); (c) $BrCH_2CO_2H$, DIC; (d) **8**, $(i\text{-}Pr)_2NEt$; (e) TFA/H_2O/EDT (95:2.5:2.5); (f) NH_4OH (air oxidation); (g) $InCl_3$. *Abbreviations:* Mtt: 4-methyltrityl; Cit: L-citrulline, Nal: L-3-(2-naphthyl)alanine, 4FBz: 4-fluorobenzoyl.

2.3. Bioactivity of In-DTPA-labeled CXCR4 antagonists

The biological activity of the In-DTPA-labeled peptides **27a–c** was evaluated as the inhibitory potency of [^{125}I]-SDF-1-binding to CXCR4 membrane extracts (Scheme 4). Peptides **27a,b**, with an N-terminal acetyl group, exhibited similar potency towards CXCR4 [IC_{50}(**27a**) = 1.95 ± 0.64 μM, IC_{50}(**27b**) = 1.60 ± 0.91 μM], indicating that the Lys and Arg for the *i*-position of β-turn were both tolerant to the bioactivity. In contrast, peptide **27c** exerted much more potent inhibitory activity for the SDF-1 binding to CXCR4 [IC_{50}(**27c**) = 0.014 ± 0.010 μM]. These results of In-DTPA-labeled peptides **27a–c** coincided with our previous report on the unlabeled peptides.[28] The novel potent In-DTPA-labeled CXCR4 antagonist **27c** could be a promising imaging probe for CXCR4-expressing malignant cancer cells.[11]

3. Conclusions

In this study, we have established a novel synthetic method for the production of DTPA–peptide conjugates. The process includes facile solid-phase synthesis of a DTPA framework using a novel precursor substrate and site-specific conjugation using a highly acid-labile protecting group. Using a temporary Ns protecting group, the DTPA precursor **8** was obtained through two purification steps from commercially available diethylenetriamine. In addition, the on-resin incorporation of a bromoacetyl group into the specific free amino group followed by the addition of the nucleophilic DTPA precursors provided the expected DTPA–peptide conjugates with high purity. Taking advantage of secondary amine precursors of choice, these processes represent versatile methods to prepare a series of peptide conjugates, including DTPA and DOTA, for optimization of imaging probes. This conjugation method was applied to the preparation of DTPA-conjugates of octreotide and CXCR4 antagonist, which have been reported to effectively detect cancer cells. The peptide **27c** with highly potent inhibitory activity of SDF-1 binding to CXCR4 was obtained without any amino acid substitution to avoid multiple modifications on the amino groups. This peptide represents a promising lead compound as an imaging probe towards CXCR4-positive metastatic tumors.

4. Experimental

4.1. Synthesis

4.1.1. Bis(*tert*-butyl) 3,6-bis[(*tert*-butoxycarbonyl)methyl]-9-(*o*-nitrobenzenesulfonyl)-3,6,9-triazaundecanedioate (14a)

To diethylenetriamine **5** (0.540 mL, 5.00 mmol) in dehydrated EtOH (5 mL), *o*-NsCl (0.367 g, 1.67 mmol) was slowly added below 0 °C. After stirring for 2 h, EtOH was removed in vacuo. To dehydrated DMF (8 mL), K_2CO_3 (4.49 g, 32.5 mmol) and $BrCH_2CO_2t$-Bu (4.06 mL, 27.5 mmol) were added at 0 °C. The mixture was stirred overnight at room temperature, and filtered. The filtrate was concentrated under reduced pressure to give an oily residue, and the residue was dissolved in EtOAc (100 mL). The whole mixture was washed with saturated $NaHCO_3$, and was dried over $MgSO_4$. Concentration under reduced pressure followed by flash chromatography over silica gel with *n*-hexane–EtOAc gave compound **14a** as a yellow oil (0.81 g, 65%); ^{1}H NMR ($CDCl_3$, 500 MHz) δ 8.08–8.11 (1H, m), 7.64–7.69 (2H, m), 7.56–7.60 (1H, m), 4.24 (2H, s), 3.49 (2H, t, *J* = 6.9 Hz), 3.42 (4H, s), 3.30 (2H, s), 2.88 (2H, t, *J* = 6.6 Hz), 2.78 (2H, t, *J* = 6.9 Hz), 2.77 (2H, t, *J* = 6.9 Hz), 1.45 (27H, s), 1.36 (9H, s); ^{13}C NMR ($CDCl_3$, 500 MHz) δ 170.6 (3C), 168.0, 133.7, 133.2, 131.6 (2C), 130.9, 123.9, 82.0, 81.0, 80.9 (2C), 56.1 (3C), 53.3, 52.8, 52.4, 49.4, 46.7, 28.1 (9C), 27.9 (3C); HRMS (FAB) *m/z* calcd for $C_{34}H_{58}N_4O_{12}S$ ([M+H]$^+$): 746.3772, found 746.3779.

4.1.2. Bis(*tert*-butyl) 3,6-bis[(*tert*-butoxycarbonyl)methyl]-3,6,9-triazaundecanedioate (8)

To a solution of compound **14a** (0.216 g, 0.29 mmol) in DMF (0.726 mL), LiOH (0.128 g, 2.90 mmol) and mercaptoacetic acid (0.101 mL, 1.45 mmol) were added below 0 °C. After stirring for 2 h at room temperature, the mixture was concentrated under reduced pressure, and the residue was dissolved in $CHCl_3$. The whole reaction mixture was washed with saturated $NaHCO_3$, and was dried over Na_2SO_4. Concentration under reduced pressure followed by flash chromatography over silica gel with $CHCl_3$–MeOH gave compound **8** as a yellow oil (0.124 g, 77%); ^{1}H NMR ($CDCl_3$, 500 MHz) δ 3.39 (4H, s), 3.28 (4H, s), 2.72–2.82 (6H, m), 2.63 (2H, t, *J* = 5.4 Hz), 1.39 (9H, s), 1.38 (27H, s); ^{13}C NMR ($CDCl_3$, 500 MHz) δ 170.9, 170.7 (3C), 80.8 (4C), 55.9 (2C), 55.8 (2C), 52.4, 52.3, 51.3, 47.0, 28.2 (3C), 28.1 (9C); HRMS (FAB) *m/z* calcd for $C_{28}H_{54}N_3O_8$ ([M+H]$^+$): 560.3911, found 560.3910.

4.1.3. Standard procedure for solid-phase peptide synthesis

Protected peptide-resins were manually constructed by Fmoc-based solid-phase peptide synthesis. *t*-Bu ester for Asp and Glu; 2,2,4,6,7-pentamethyldihydrobenzofurane-5-sulfonyl (Pbf) for Arg; *t*-Bu for Thr and Tyr; Boc for Lys and Trp; Trt for Cys were employed for side-chain protection. Fmoc-amino acids were coupled using three equivalents of reagents [Fmoc-amino acid, 1,3-diisopropylcarbodiimide (DIC), and HOBt·H_2O] to the free amino group in DMF for 1.5 h. Fmoc deprotection was performed by 20% (v/v) piperidine in DMF (2 × 1 min, 1 × 30 min). The protected peptide resin was treated with a cocktail of deprotection reagents. After removal of the resin by filtration, the filtrate was poured into ice-cold dry Et_2O. The resulting powder was collected by centrifugation and washed with ice-cold dry Et_2O. The crude peptide was dissolved in H_2O, and the pH was adjusted to 8.0 with NH_4OH for disulfide bond formation. After air-oxidation for 1 d, the crude product was purified by preparative HPLC on a Cosmosil 5C18-ARII preparative column (Nacalai Tesque, Kyoto, Japan; 20 × 250 mm, flow rate 10 mL/min) to afford the expected peptides. All peptides were characterized by MALDI-TOF-MS (AXIMA-CFR plus, Shimadzu, Kyoto, Japan) and the purity was calculated as >95% by HPLC on a Cosmosil 5C18-ARII analytical column (Nacalai Tesque, 4.6 × 250 mm, flow rate 1 mL/min) at 220 nm absorbance.

4.1.4. Preparation of DTPA- and DOTA-conjugated octreotides (19a,b)

According to the procedure reported previously,[18] (2-chloro)trityl chloride resin **15** (214 mg, 1.4 mmol/g), Fmoc-Thr(*t*-Bu)-ol (345 mg, 0.9 mmol), and pyridine (0.145 mL, 1.8 mmol) were agitated for 21 h in dry CH_2Cl_2–DMF (1:1, 3.94 mL). The loading was determined by measuring the 290 nm UV absorption of the piperidine-treated sample (0.455 mmol/g). After the construction of the peptide chain (0.017 mmol scale) using a standard procedure, bromoacetic acid (23.6 mg, 0.17 mmol) with DIC (0.026 mL, 0.17 mmol) in CH_2Cl_2 was reacted with resin **16** for 2 h at room temperature. The subsequent treatment of **17** with amines **8** (29.0 mg, 0.51 mmol) and **20** (26.3 mg, 0.51 mmol) with $(i\text{-Pr})_2$NEt (0.009 mL, 0.51 mmol) in DMF for 12 h at room temperature provided **18a** and **18b**, respectively. Cleavage and deprotection of **18a** (72.5 mg) and **18b** (73.8 mg) was achieved using a TFA/1,2-ethandithiol (EDT)/H_2O (5 mL; 95:2.5:2.5) cocktail for 2 h at room temperature and by treatment with 1 M TMSBr-thioanisole/TFA in the presence of EDT/*m*-cresol (3.3 mL) for 2 h at 0 °C, respectively. After disulfide formation under air-oxidation conditions, the crude peptides were purified using the standard procedure, to afford the desired peptides **19a** (8.2 mg, 23%) and **19b** (9.5 mg, 26%) as white powders. Compound **19a**: MS (MALDI-TOF) *m/z* calcd for $C_{63}H_{89}N_{13}O_{19}S_2$ ([M+H]$^+$): 1395.6, found 1395.3. Compound **19b**:

MS (MALDI-TOF) *m/z* calcd for $C_{65}H_{93}N_{14}O_{17}S_2$ ($[M+H]^+$): 1405.6, found 1405.8.

4.1.5. Preparation of DTPA-conjugated CXCR4 antagonists (26a–c)

Protected peptide resins were manually constructed according to the standard procedure using NovaSyn TGR-resin **21** (96.2 mg, 0.025 mmol). 4-Methyltrityl (Mtt) group was employed for the protection of the D-Lys ε-amino group. The N-terminal amino group was acylated by treatment with Ac_2O (0.012 mL, 0.125 mmol)/pyridine (0.020 mL, 0.250 mmol) for 1 h at room temperature for peptides **26a,b**, and with 4-fluorobenzoic acid (17.5 mg, 0.125 mmol)/DIC (0.019 mL, 0.125 mmol)/HOBt·H_2O (19.2 mg, 0.125 mmol) for 1.5 h at room temperature for peptide **26c**. Subsequently, the resin **22** was treated with CH_2Cl_2/1,1,1,3,3,3-hexafluoropropan-2-ol (HFIP)/trifluoroethanol (TFE)/triethylsilane (TES) [65:20:10:5; 5 mL] for 2 h at room temperature. The DTPA group was incorporated using the identical procedure employed for the synthesis of the octreotide derivative **19a**. Treatment of the resins (**25a**: 178 mg, **25b**: 165 mg, **25c**: 162 mg) with a TFA/1,2-ethandithiol(EDT)/H_2O (95:2.5:2.5; 5 mL) cocktail for 2 h at room temperature followed by air oxidation and purification provided the peptides Compound **26a** (14.6 mg, 15.4%), **26b** (6.67 mg, 8.7%) and **26c** (7.4 mg, 9.5%) as white powders. Compound **26a:** MS (MALDI-TOF) *m/z* calcd for $C_{106}H_{165}N_{38}O_{28}S_2$ ($[M+H]^+$): 2482.2, found 2482.5. Compound **26b**: MS (MALDI-TOF) *m/z* calcd for $C_{106}H_{165}N_{36}O_{28}S_2$ ($[M+H]^+$): 2454.2, found 2453.9. Compound **26c**: MS (MALDI-TOF) *m/z* calcd for $C_{111}H_{166}FN_{36}O_{28}S_2$ ($[M+H]^+$): 2534.2, found 2533.8.

4.1.6. Indium chelating for CXCR4 antagonist probes (27a–c)

To a solution of peptides **26a–c** (8 mM in 0.1 N AcOH, **26a**: 45.9 μL, 0.37 μmol; **26b**: 48.4 μL, 0.39 μmol; **26c**: 48.8 μL, 0.39 μmol), $InCl_3$ (1 M in 0.02 N HCl, 50 μL) was added and the solution stirred for a further 30 min at room temperature. HPLC purification using a standard procedure provided the desired peptides **27a** (0.43 mg, 36.7%), **27b** (0.42 mg, 34.3%) and **27c** (0.38 mg, 30.3%) as white powders. Compound **27a**: MS (MALDI-TOF) *m/z* calcd for $C_{106}H_{165}InN_{38}O_{28}S_2$ ($[M+H]^+$): 2597.1, found 2596.9. Compound **27b**: MS (MALDI-TOF) *m/z* calcd for $C_{106}H_{165}InN_{36}O_{28}S_2$ ($[M+H]^+$): 2569.1, found 2569.1. Compound **27c**: MS (MALDI-TOF) *m/z* calcd for $C_{111}H_{166}FInN_{36}O_{28}S_2$ ($[M+H]^+$): 2649.1, found 2649.0.

4.2. Evaluation of [^{125}I]-SDF-1 binding and displacement

For ligand binding, the CXCR4 membrane was incubated with 0.5 nM of [^{125}I]-SDF-1 and increasing concentrations of compounds **27a–c** in binding buffer [50 mM HEPES (pH 7.4), 5 mM $MgCl_2$, 1 mM $CaCl_2$ and 0.1% BSA in H_2O] for 1 h at room temperature. The reaction mixtures were filtered through GF/B filters (Perkin-Elmer, Wellesley, MA) pretreated with 0.1% polyethyleneimine. The filter plate was washed with wash buffer [50 mM HEPES (pH 7.4), 500 mM NaCl and 0.1% BSA in H_2O] and the bound radioactivity was measured by TopCount (Packard, Meriden, CT). Inhibitory activity of test compounds was determined based on the inhibition of [^{125}I]-SDF-1 binding to the CXCR4 receptor (IC_{50}).

Acknowledgments

This work is supported by Grants-in-Aid for Scientific Research and Molecular Imaging Research Program from the Ministry of Education, Culture, Sports, Science, and Technology of Japan. R.M. is grateful for Research Fellowships from the JSPS for Young Scientists.

Supplementary data

Supplementary data associated with this article can be found, in the online version, at doi:10.1016/j.bmc.2011.03.059.

References and notes

1. Lee, S.; Xie, J.; Chen, X. *Chem. Rev.* **2010**, *110*, 3087.
2. De León-Rodríguez, L. M.; Kovacs, Z. *Bioconjugate Chem.* **2008**, *19*, 391.
3. Mier, W.; Hoffend, J.; Krmer, S.; Schuhmacher, J.; Hull, W. E.; Eisenhut, M.; Haberkorn, U. *Bioconjugate Chem.* **2005**, *16*, 237.
4. Lewis, M. R.; Shively, J. E. *Bioconjugate Chem.* **1998**, *9*, 72.
5. Heppeler, A.; Froidevaux, S.; Mäcke, H. R.; Jermann, E.; Powell, P.; Henning, M. *Chem. Eur. J.* **1999**, *5*, 1974.
6. De León-Rodriguez, L. M.; Kovacs, Z.; Dieckmann, G. R.; Sherry, A. D. *Chem. Eur. J.* **2004**, *10*, 1149.
7. Wild, D.; Wicki, A.; Mansi, R.; Béhé, M.; Keil, B.; Bernhardt, P.; Christofori, G.; Ell, P. J.; Mäcke, H. R. *J. Nucl. Med.* **2010**, *51*, 1059, and the references therein.
8. De Jong, M.; Breeman, W. A.; Bakker, W. H.; Kooij, P. P.; Bernard, B. F.; Hofland, L. J.; Visser, T. J.; Srinivasan, A.; Schmidt, M. A.; Erion, J. L.; Bugaj, J. E.; Mäcke, H. R.; Krenning, E. P. *Cancer Res.* **1998**, *58*, 437.
9. Hnatowich, D. J.; Layne, W. W.; Childs, R. L. *Int. J. Appl. Radiat. Isot.* **1982**, *33*, 327.
10. Wang, S.; Luo, J.; Lantrip, D. A.; Waters, D. J.; Mathias, C. J.; Green, M. A.; Fuchs, P. L.; Low, P. S. *Bioconjugate Chem.* **1997**, *8*, 673.
11. Reilly, R.; Lee, N.; Houle, S.; Law, J.; Marks, A. *Appl. Radiat. Isot.* **1992**, *43*, 961.
12. Hnatowich, D. J.; Layne, W. W.; Childs, R. L.; Lanteigne, D.; Davis, M. A.; Griffin, T. W.; Doherty, P. W. *Science* **1983**, *220*, 613.
13. Van Hagen, P. M.; Breeman, W. A. P.; Bernard, H. F.; Schaar, M.; Mooij, C. M.; Srinivasan, A.; Schmidt, M. A.; Krenning, E. P.; De Jong, M. *Int. J. Cancer* **2000**, *90*, 186.
14. Arano, Y.; Uezono, T.; Akizawa, H.; Ono, M.; Wakisaka, K.; Nakayama, M.; Sakahara, H.; Konishi, J.; Yokoyama, A. *J. Med. Chem.* **1996**, *39*, 3451.
15. A portion of this study was reported in a preliminary communication: Masuda, R.; Ohno, H.; Oishi, S.; Fujii, N. In *Pepide Science*, Okamoto, Ed.; 2009, p 159.
16. Peterson, J. J.; Pak, R. H.; Meares, C. F. *Bioconjugate Chem.* **1999**, *10*, 316.
17. Hidai, Y.; Kan, T.; Fukuyama, T. *Chem. Pharm. Bull.* **2000**, *48*, 1570.
18. Arano, Y.; Akizawa, H.; Uezono, T.; Akaji, K.; Ono, M.; Funakoshi, S.; Koizumi, M.; Yokoyama, A.; Kiso, Y.; Saji, H. *Bioconjugate Chem.* **1997**, *8*, 442.
19. Lewis, J. S.; Anderson, C. J. *Methods Mol. Biol.* **2007**, *386*, 227.
20. Albert, R.; Smith-Jones, P.; Stolz, B.; Simeon, C.; Knecht, H.; Bruns, C.; Pless, J. *Bioorg. Med. Chem. Lett.* **1998**, *8*, 1207.
21. Müller, A.; Homey, B.; Soto, H.; Ge, N.; Catron, D.; Buchanan, M. E.; McClanahan, T.; Murphy, E.; Yuan, W.; Wagner, S. N.; Barrera, J. L.; Mohar, A.; Verástegui, E.; Zlotnik, A. *Nature* **2001**, *410*, 50.
22. Hermann, P. C.; Huber, S. L.; Heeschen, C. *Cell Cycle* **2008**, *7*, 188.
23. Oishi, S.; Masuda, R.; Evans, B.; Ueda, S.; Goto, Y.; Ohno, H.; Hirasawa, A.; Tsujimoto, G.; Wang, Z.; Peiper, S. C.; Naito, T.; Kodama, E.; Matsuoka, M.; Fujii, N. *ChemBioChem* **2008**, *9*, 1154.
24. Nishizawa, K.; Nishiyama, H.; Oishi, S.; Tanahara, N.; Kotani, H.; Mikami, Y.; Toda, Y.; Evans, B. J.; Peiper, S. C.; Saito, R.; Watanabe, J.; Fujii, N.; Ogawa, O. *Int. J. Cancer* **2010**, *127*, 1180.
25. Hanaoka, H.; Mukai, T.; Tamamura, H.; Mori, T.; Ishino, S.; Ogawa, K.; Iida, Y.; Doi, R.; Fujii, N.; Saji, H. *Nucl. Med. Biol.* **2006**, *33*, 489.
26. Tamamura, H.; Omagari, A.; Oishi, S.; Kanamoto, T.; Yamamoto, N.; Peiper, S. C.; Nakashima, H.; Otaka, A.; Fujii, N. *Bioorg. Med. Chem. Lett.* **2000**, *10*, 2633.
27. Stephenson, K. A.; Banerjee, S. R.; McFarlane, N.; Boreham, D. R.; Maresca, K. P.; Babich, J. W.; Zubieta, J.; Valliant, J. F. *Can. J. Chem.* **2005**, *83*, 2060.
28. Tamamura, H.; Hiramatsu, K.; Mizumoto, M.; Ueda, S.; Kusano, S.; Terakubo, S.; Akamatsu, M.; Yamamoto, N.; Trent, J. O.; Wang, Z.; Peiper, S. C.; Nakashima, H.; Otaka, A.; Fujii, N. *Org. Biomol. Chem.* **2003**, *1*, 3663.